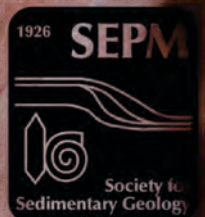


THE VOLUME 19, NO. 2 | JUNE 2021 SEDIMENTARY RECORD

A PUBLICATION BY THE SOCIETY FOR SEDIMENTARY GEOLOGY

doi: 10.2110/sedred.2021.1



Editors

Jenn Pickering
Jeong-Hyun Lee
Howard Harper

SEPM | Society for Sedimentary Geology

1621 S. Eucalyptus Ave.
Suite 204,
Broken Arrow, OK 74012
sepm.org

Cover image:

Copyright - Felicia Lynne
Lee | [https://felicialee.
smugmug.com/](https://felicialee.smugmug.com/)



Table of Contents

SUSTAINABILITY WITHOUT GEOLOGY? A SHORTSIGHTED APPROACH

Andrea Fildani and Angela M. Hessler

1 - 4

OVERNIGHT FORMATION OF A BOULDERY ALLUVIAL FAN BY A TORRENTIAL RAIN IN A GRANITIC MOUNTAIN (MT. SEORAKSAN, REPUBLIC OF KOREA)

Jisu Kim, Kyung Sik Woo, Kwang Choon Lee and Young Kwan Sohn

5 - 11

IDENTIFYING ELUSIVE PIERCING POINTS ALONG THE NORTH AMERICAN TRANSFORM MARGIN USING MIXTURE MODELING OF DETRITAL ZIRCON DATA FROM SEDIMENTARY UNITS AND THEIR CRYSTALLINE SOURCES

J. Clark Gilbert, Zane R. Jobe, Samuel A. Johnstone and Glenn R. Sharman

12 - 21 | Supplementary Material 22 - 31

doi:10.2110/sedred.2021.1

ISSN 1543-8740

Attribution-NonCommercial 4.0 International (CC BY-NC 4.0)

Sustainability without Geology? A Shortsighted Approach

Andrea Fildani^{1,*} and Angela M. Hessler¹

¹The Deep Time Institute, 13809 Research Boulevard, Suite 500 94952, Austin, Texas 78750, USA

There are no beautiful surfaces without a terrible depth.
—F. W. Nietzsche

Over the last few decades, the concept of *sustainability* has been proposed and championed as the answer to the impending challenges our society will be facing in the future. It has been a rallying opportunity for the broad earth sciences community and a good starting point for such a community to impact societal and policy decisions; however, it has been an opportunity we have largely missed thus far. We are not the first to notice that the sustainability wave has left geosciences behind. In fact, almost ten years ago, Grimm and Van Der Pluijm (2012) lamented the absence of geoscientists at a National Academies Symposium aimed at “Science, Innovation, and Partnerships for Sustainable Solutions.”

Sustainability theory is rooted in three interconnected domains or pillars: social, economic, and environmental sustainability. Much of the early notion stemmed from the United Nations’ initiatives where the basic concepts were sharpened over the last 50 years (see Purvis et al., 2019, for a review of concepts through time). The anticipation is that the three pillars, if properly harmonized, will improve both the present and future potential to meet human needs and aspirations (<https://sdgs.un.org/goals>). So, it is often stated that the main drive behind sustainability—and its corollary initiatives—is to explore the capacity for the biosphere and human civilization to co-exist, in which the term (sustainability) is thrown around as the *deus ex machina* that will, if correctly implemented, save us and our planet. While it is important for humans to act upon the foreseeable changes to our planet with urgent mitigation—such as the upcoming climate crisis—we fear that the current strategies are too shortsighted and anthropocentric to produce durable solutions. This may be because sustainability education and research are taking place in the absence of geological sciences, and without

deep familiarity with Earth’s history and dynamism, these efforts will fall short in protecting our future.

The word *sustainability* is one of the most used words in the current scientific vocabulary (<https://xkcd.com/1007/>). In fact, by the end of this paper, you will have read the word another 36 times. It has been so overused (or abused) in appropriate and inappropriate ways that it has many critics who find the word vague or nonspecific. We think that the word could be appropriate in the right context but has been haphazardly applied due to a major philosophical gap in most sustainability efforts.

We can start with an etymological dig into the original meaning of the word. Sustainability derives from the Latin word *sustinēre*, formed by *sus-*, a variant of *sub-* meaning “under” and *tenere*, meaning “hold”. Therefore, the epistemological meaning of the word is to “hold under”. Considering how human-centric we tend to be in our society, one interpretation of the word could be to “hold under” nature to sustain the needs of an overgrowing society. Maybe a more suitable (friendly?) interpretation would be to “hold”—*tenere*—something to a certain level, to a standard, a potentially ideal datum to which to aspire or regress (in the case of overgrowth).

But what is our *standard*? Our *datum*? As scientists, we feel the need to define what and how we are measuring and from which baseline. Agreements on the standard to achieve (if we use CO₂ levels) often point toward conditions just prior to the Industrial Revolution. However, because humans have been modifying the environment for the last 8000 years (Ruddiman, 2005), why not aim further back in time to the end of the Last Glacial? Or the appearance of *Homo erectus*? And how do we honor natural change? Our society is a mere eye-blink in geologic time; settling on a datum must reckon with this fact.

We make the point that every initiative in sustainability and any theoretical application of it should not (and cannot) be enabled without the full consideration of deep time that only earth scientists can bring to the table. This shares some similarities with the concept of a “deep time reckoning”

introduced by Ialenti (2020) but modified to apply longer temporal perspectives or “timefulness” (Bjornerud, 2018) in using the past as an indispensable framework for the future.

Since the world’s richest and most privileged people are now throwing their money behind climate engineering (maybe without fully grasping the concept), we think geologic principles should be implemented swiftly to prevent yet more unforeseen consequences. One place to start is at the university level, where sustainability programs are proliferating to the exclusion of earth sciences, with a few timid exceptions.

A HISTORICAL SCIENCE: THE PAST ENLIGHTENS THE PRESENT TO GUIDE OUR FUTURE

We are members of an observation-based historical science; this should be viewed as an advantage and a privilege—nobody can see the world as we can. Unfortunately, those with environmental policy power and market power are not necessarily asking for our advice.

Of the three theoretical pillars of sustainability, the environmental pillar seems to be the one most logically aligned with earth sciences. It makes sense that this pillar should be strongly rooted in the disciplines that study and understand Earth, its past, its climate fluctuations, and its profound transformation through time. Unfortunately, that is not always the case. Depending on the search engine and wording used in one’s browsing, the results consistently suggest the lack in depth in geosciences. The top geology programs in the USA are responding differently to the external push in this direction. While some departments have added “environmental” to their names (this has been going on for decades), the involvement of some geoscience departments with neighboring sustainability initiatives go from inaction (hence missing the opportunity) to acknowledgment (upon donors’ pressure) but still hesitant impasse, to the complete surrender of their programs to the new trend.

Some universities have established pathways for students to receive undergraduate and/or graduate degrees in sustainability (sometimes tagged as environmental sciences or earth systems) in juxtaposition with earth science departments or schools. But perhaps due to the Venn-like relationship between the three pillars and the vagueness of the central concept, these academic programs are a maze of core and elective classes that flit around social sciences, statistics, economics, biology/chemistry, physics, and policy, depending on the chosen specialty track. The most inspired departments might graduate students in sustainability or earth systems with a requirement of one (only 1!) class in earth or natural sciences; and such a class could be a field trip or a farming experience or entirely about ecosystems. We surveyed 40 high-ranking U.S. degree programs in sustainability (or environmental science) and found that only nine required geology in at least one of their tracks, and of those only three required more than one course (Fig. 1). Geology courses are included on most elective

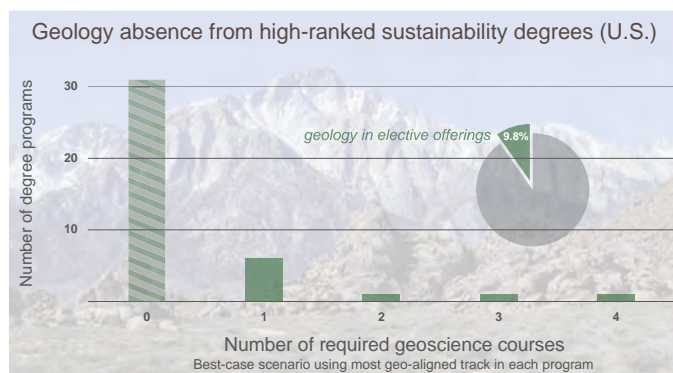


Figure 1: The number of required geoscience courses, and the percent geoscience electives, in 40 sustainability or environmental science undergraduate programs in the U.S. These programs typically offer multiple tracks; the data here represent the curricula from the most geoscience-relevant track in each program. Where given a choice, we surveyed the Bachelor of Science degree program. The programs represent a wide geographic range of public, private, and small- and large-population colleges and universities and were listed as top-ranking environmental or sustainability programs at: www.universities.com, www.usnews.com, www.bestvalueschools.com, or www.environmentalscience.org. The three schools requiring more than one geoscience course include the University of Vermont, University of South Dakota, and Stanford University.

lists, but even so, they are so swamped by other offerings that geology courses make up on average less than 10% of all electives (Fig. 1). If students are lucky (and maybe well-advised) they might be exposed to something like Global Climate Change Sciences, which some programs are far-sighted enough to include in their course list. However, Earth History, shockingly enough, is not listed as a mandatory class in many programs. It is fairly easy for students to receive a degree in policy or economics or even land use under the large umbrella of sustainability without being exposed to earth sciences.

While it is always dangerous to generalize and, of course, there are differences among schools and programs, one cannot escape the extent of the problem. Many institutions proudly tout they are graduating the future leaders in sustainability, but they forget to mention that the students do not acquire the tools to really understand earth’s processes and past changes. Granted, opportunities to deepen one’s knowledge might be available at an individual level such that certain students can expand their geoscience experiences, but the fact that universities are focusing their sustainability training into social sciences, biological sciences, and/or engineering is shortsighted. Climate changes and their impact on our society are understood largely due to the work of geologists; seeing programs that do not keep at least Earth History and Geomorphology among their core mandatory courses is troublesome.

It is interesting to notice that European high schools and universities seems to have a more geologic-centric approach to sustainability (and geology overall), and their

programs do offer courses such as Dynamic Earth and Planetary Evolution or Earth Surface Evolution (as it responds to climatic changes). As we write this, our two sons are in public middle and high school in Italy where the science curriculum includes earth science (textbook and everything!) in straight balance with chemistry, physics, and biology. This early visibility of geology—whatever the cultural forces behind it—must make it easier for university geoscience programs to be in on the sustainability conversation.

A CONFLUENCE OF HUMAN CRISES: CLIMATE CHANGE AND INFECTIOUS DISEASES

Theoretical links between climatic fluctuations and pandemics have been postulated and discussed for a long time (see [Ruddiman, 2005](#), and its references). When the world stumbled onto SARS-CoV-2 (Severe Acute Respiratory Syndrome CoronaVirus 2) in late 2019, it should not have been such a surprise. This pandemic was a turning point and potentially the opening of Pandora's Box in that it exposes how climatic change expands the intersection between human living spaces and disease carriers, by shifting the global distribution of such carriers (e.g., [Beyer et al., 2021](#)).

The pandemic offered *per se* a daunting example with regard to crisis preparation. In the 1970s, the World Health Organization declared victory against diseases ([McNeill, 1975](#)), as it seemed the diseases that historically afflicted humans were on the retreat after decades of vaccination efforts. Unfortunately, a series of new pandemics (and a fresh new batch of viruses) swept through the world; HIV, SARS, Ebola, MERS, Ebola again and now SARS-2 are showing us how important long-term planning and prevention can be. These “new” viruses are actually old (if we carefully reconstruct the zoonosis) and they show we must have a historical perspective even in understanding societal diseases; a society is never immune in its interaction with an ever-changing nature especially when such society is modifying ecosystems at an unprecedented rate ([Quammen, 2012](#)).

[McNeill's](#) paradigm-shifting work in *Plagues and People* (1975) was an important early contribution to the study of the impact of diseases throughout human history. McNeill poses that history could be read through the lens of pandemics and not necessarily through the powers and military superiority accumulated via armies and gold. His careful review poses the balance between humans and diseases sharply in focus (wherein one might momentarily prevail over the other in a dynamic balance) offering an opportunity to explore history in a different way.

We surely took the uninvited opportunity given to us by viruses and their predominance on the world news to learn that viruses together with microbes and bacteria have been around for billions of years. Of course we should have known better that such a fundamental force in shaping the planet biota had to be involved with the development of early life on Earth ([Krupovic et al., 2019](#)). Without fully

embracing a virocentric perspective on the evolution of life, multiple lines of evidence have been presented showing the central role of viruses in the earth's entire evolution ([Koonin and Dolja, 2013](#)). There are trillions of viruses in the modern oceans, making them the most numerous biological entities in the world's oceans, profoundly regulating the deep-sea ecosystems, and marine biologists and ecologists are only recently beginning to tackle the effects of viruses on the broader ocean ecology ([Zimmer, 2015](#)). Palaeoecologists have been looking into the effects of diseases on paleoenvironments; the example of [Poinar and Poinar \(2008\)](#) on dinosaurs' paleoecology is one that comes to mind. There is plenty of room to start thinking about viruses through deep time and contemplating their impact on the evolution of life on Earth, including our own species. Cesare Emiliani, in a prescient contribution from about 30 years ago, warned us:

Indeed, both Emiliana huxley (Emiliana huxley is a species of coccolithophore) and Homo sapiens appear to be under viral attack. . . It is of course impossible to predict whether the attacks will be terminal, whether the responsible viruses will mutate themselves out of existence, or whether immunity will develop in one or both species, giving at least temporary reprieve. (Emiliani, 1993).

We think an incredible opportunity is in front of our inherently historical science; a science that tracks changes by studying the sedimentary record. If history could be read through the lens of disease (as suggested by [McNeill, 1975](#)) and extinctions could have a viral (or microbial) component to them ([Emiliani, 1993](#)), our skills as geoscientists would be helpful to the conversations about how to prepare for the future. A historical “habit of mind” is advisable for every action we undertake.

A GROUNDED EMBRACE OF OUR PLANET'S DYNAMIC DISEQUILIBRIUM

The higher we soar, the smaller we appear to those who cannot fly. –F. W. Nietzsche

Economists, philosophers, physicists, and engineers got involved early on in the debate about the future of our society and have been active in decision-making processes. They pushed the sustainability ‘boat’ straight to the highly theoretical level of system (and complex) thinking—hence fundamentally soaring it off the very *terra firma* to which complex thinking should be anchored: Earth. Sustainability should walk on foot! With the theorists of the three pillars heavily weighted toward the economic and social sciences, the environmental pillar is left behind to be mostly an engineer's afterthought.

Firstly, we need to position earth sciences as the core of the environmental pillar. To do this, we suggest emphasizing the importance of the biosphere as it is linked to the geosphere. This is not a petty fight between sciences but a philosophical need solely pointing to the exposition of

a fundamental fact. Biosphere and geosphere have constantly danced together to shape the environment we live in (as elegantly explained by Knoll, 2003). Life's evolution through its long history influenced earth's surface more than one might think and, overall, the central role of plate tectonics—arguably among the most influential revolutions of the last century—has never been fully appreciated by the general public. The role of oxygenic photosynthesis (and the appearance of large quantities of “poisonous” oxygen in the atmosphere; see Lane, 2002) and the coupled atmosphere and ocean interactions through time illustrate the complex relationship between evolution and environmental changes.

In addition to a more balanced treatment of the biosphere and geosphere, we think geomorphology is underrepresented in environmental and sustainability science training. Global landscape evolution through space and time interacts with the atmosphere and hydrosphere, reacting to any dictation of climate and its changes through time. The sedimentary record is the outcome of such interactions. How can a graduate of a sustainability program become suitably aware of landscape change without taking classes in earth history and geology? And then how will this graduate help mitigate the distress of coastal communities related to sea-level rise, or understand the full range of possibilities in terms of flood patterns or erosion rates?

The notion that the planet's habitability, as it is nowadays, which fostered the rise of our species, was somehow given to humans as our perfectly designed living place is plain wrong. As earth scientists know, the evolution of Earth from its early days has been a winding path, a long great adventure of which we are sorting out the details thanks to the incredible amount of work done by many colleagues over the last few centuries. Fundamental understanding of critical geological phenomena on Earth must be used to solve scientific, engineering, and societal challenges around our future survival. Furthermore, the resilience of global landscapes during a time of rapid perturbations appears to be the one major control on anything we do to mitigate the changes to come. There is the unsettling feeling that many of the “corrective means” brought up by sustainability studies are more short-term engineering mitigations rather than long-term solutions. Some brute force attempts to control our climate (e.g., carbon removal) bear unpredictable risks via poorly understood feedbacks within the oceans and biosphere. Most of us are aware that the engineering of nature comes with unintended consequences, high costs, and even higher stakes for the society directly impacted (see *The Control of Nature* by McPhee, 1989).

THE OPPORTUNITY

Our planet is in a constant *dynamic disequilibrium*, and within such a state we need to learn how to coexist. This fundamental concept should shape the leadership of the future so that mitigation attempts are not fragile engineering maneuvers pushed upon nature (or editorial stunts by

big personalities) but instead are durable solutions that can adapt to forecasted feedbacks and out-of-normal events. Maybe the sustainability camp has been clever at advertising their cause, and maybe geologists have not done such a good job at enticing the public opinion, but we think that attracting well-meaning students into career paths that do not have adequate grounding in earth sciences could be unfortunate for our society (and for the future of such students). For this reason, earth science must be promoted and presented as a core value in the sustainability programs that are now growing across universities.

To us, this is an ethical call. We cannot let our society move forward with energy and economic plans without understanding the behavior and limits of the environment we are trying to sustain. Our unique and hard-earned understanding of the past must educate global decisions about climate and energy, and so we have to speak up.

Faber est suae quisque fortunae. –Appio Claudio Cieco

References

- Beyer, R. M., Manica, A., and Mora, C. (2021). Shifts in global bat diversity suggest a possible role of climate change in the emergence of SARS-CoV-1 and SARS-CoV-2. *Science of The Total Environment*, 767:145413.
- Bjornerud, M. (2018). *Timefulness*. Princeton University Press.
- Emiliani, C. (1993). Extinction and viruses. *Biosystems*, 31(2-3):155–159.
- Grimm, N. and Van Der Pluijm, B. (2012). Sustainability needs the geosciences. *EOS*, 93(44):441.
- Ialenti, V. (2020). *Deep Time Reckoning: How Future Thinking Can Help Earth Now*. MIT Press.
- Knoll, A. H. (2003). The geological consequences of evolution. *Geobiology*, 1(1):3–14.
- Koonin, E. V. and Dolja, V. V. (2013). A virocentric perspective on the evolution of life. *Current opinion in virology*, 3(5):546–557.
- Krupovic, M., Dolja, V. V., and Koonin, E. V. (2019). Origin of viruses: primordial replicators recruiting capsids from hosts. *Nature Reviews Microbiology*, 17(7):449–458.
- Lane, N. (2002). *Oxygen: the molecule that made the world*. Oxford University Press, USA.
- McNeill, W. (1975). *Peoples and Plagues*. Anchor Books.
- McPhee, J. (1989). *The control of nature*. Farrar, Straus & Giroux, New York.
- Poinar, G. J. and Poinar, R. (2008). *What Bugged the Dinosaurs?: Insects, Disease, and Death in the Cretaceous*. Princeton University Press.
- Purvis, B., Mao, Y., and Robinson, D. (2019). Three pillars of sustainability: in search of conceptual origins. *Sustainability Science*, 14(3):681–695.
- Quammen, D. (2012). *Spillover: Animal Infections and the Next Human Pandemic*. WW Norton & Company.
- Ruddiman, W. F. (2005). *Plows, Plagues, and Petroleum: How Humans took Control of Climate*. Princeton University Press.
- Zimmer, C. (2015). *A Planet of Viruses*. The University of Chicago Press.

Overnight formation of a bouldery alluvial fan by a torrential rain in a granitic mountain (Mt. Seoraksan, Republic of Korea)

Jisu Kim¹, Kyung Sik Woo², Kwang Choon Lee³ and Young Kwan Sohn^{1,*}

¹Department of Geology and Research Institute of Natural Science, Gyeongsang National University, Jinju 52828, Republic of Korea

²Department of Geology, Kangwon National University, Chuncheon 24341, Republic of Korea

³Department of New Energy and Resource Engineering, Sangji University, Wonju 26339, Republic of Korea

ABSTRACT Mt. Seoraksan, Korea, is a rugged granitic mountain where extremely steep slopes and strongly seasonal rainfall have facilitated bedrock exposure and geomorphic changes mainly by rockfalls and streamflows. Although the environment was not suitable for alluvial fan formation, a bouldery alluvial fan, 170 m long and 330 m wide, formed overnight by a heavy summer rain in 2006. The fan consists of several meter-high boulder mounds and gently undulating cobble bars/sheets that are arranged in a fluvial longitudinal bar-like pattern. They are interpreted to have formed by highly competent and turbulent sheetfloods, which temporarily had the properties of hyperconcentrated flood flows. Formation of the whole alluvial fan by a single, casual hydro-meteorological event is inferred to have been possible because a threshold condition was reached in the source area. A rainfall event, which would have had no extreme effects before reaching the threshold, could probably trigger massive remobilization of bouldery sediments on the valley floors. The Seoraksan alluvial fan thus demonstrates the role of a geomorphic threshold in causing drastic changes in the hydrologic performance of the watershed. The morphology and sedimentology of the Seoraksan alluvial fan suggest that the fan is a modern example of a sheetflood-dominated alluvial fan, which has largely been ignored in spite of their potential diversity and abundance in glacial to periglacial, tropical, and temperate environments.

KEYWORDS alluvial fan, geomorphic threshold, sheetflood, debris flow, boulder mound

INTRODUCTION

Alluvial fans occur in diverse settings, from humid to arid regions and from tectonically active mountain fronts to stable footslopes and valley junctions. Their morphology and sedimentology are determined by the availability of water and the amount and type of sediment, which are in turn controlled by the tectonics, climate, and bedrock lithology in the catchment area (Bull, 1977, Blair and McPherson, 1994, McDonald et al., 2003). Catastrophic storms or intense rainfalls, which can occur independently of climate change and tectonic activity, also play a significant role in forming alluvial fans (Wells and Harvey, 1987, Marchi et al., 2009, Cabré et al., 2020), in some cases giving greater impacts than earthquakes (LaHusen et al., 2020). Deposition on alluvial fans can be very infrequent and inconstant. Sheetfloods and debris flows can deposit significant volumes of sediment within hours (Wells and Harvey, 1987), whereas streamflows can erode or rework the surficial sediments for over tens to hundreds of years (Harvey,

2007). In spite of a number of studies on alluvial fans, interpreting their formative processes is challenging because of the extreme variability of the frequency and magnitude of processes and the roles of multiple controlling factors. In particular, the lack of careful documentation of single geological or hydro-meteorological events in diverse settings makes it difficult to develop sedimentological models that can be applied to diverse types of alluvial fans. In this paper, we introduce a bouldery alluvial fan that was formed overnight during an intense rainfall in a granitic mountain of Korea in 2006. Based on field surveying in 2020 and comparative analysis of aerial photographs taken over a decade, we discuss the processes and controls of alluvial fan formation in a humid-temperate region affected by the Asian Monsoon, and highlight the role of intrinsic geomorphic processes in forming an alluvial fan.

SITE CHARACTERISTICS

Mt. Seoraksan is a national park of South Korea, belonging to a coastal mountain range that runs along the eastern side of the Korean Peninsula (Fig. 1A). It is characterized by sharp-crested ridges and deeply incised valleys (Fig. 1B) with the highest peak rising to 1,708 m a.s.l. The mountain is built predominantly of Proterozoic to Meso-

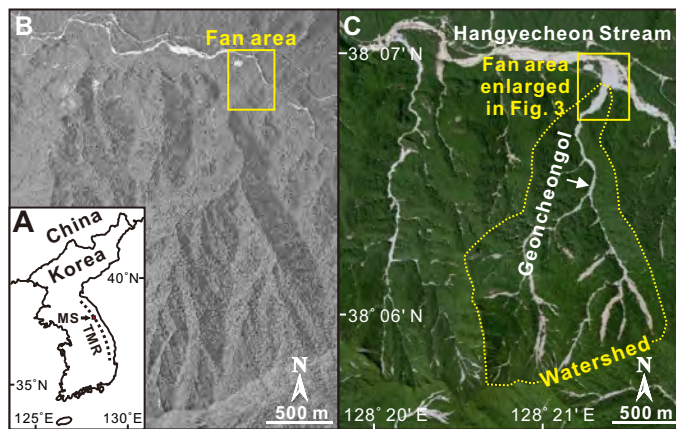


Figure 1: Location of the study area. **A:** Location of Mt. Seoraksan (MS) and the Taebaeksan Mountain Range (TMR). **B:** The study area, located in the southwestern sector of the national park area, was well-vegetated from crests to valley floors in 2005. **C:** The light-colored granitic bedrocks are exposed along the trunk and tributary valleys in 2008 (Photographs B and C are available at <http://www.ngii.go.kr> and <http://map.kakao.com>, respectively).

zoic granites (Kee et al., 2010), which are inferred to have been uplifted at a rate of ca. 0.1 mm/yr since the Cretaceous (Cho, 1994). Five earthquakes have been recorded since 1978, the largest of which had a magnitude of 2.3, according to Korea Meteorological Administration data (<https://www.kma.go.kr>). The height difference between crest lines and valley floors reaches over 1,000 m over a few km, resulting in extremely steep slopes in excess of 30–50° (Migoñ et al., 2019). Annual precipitation ranges between 800 and 1700 mm (Fig. 2A), most of which falls as heavy summer rains between June and September with daily intensities of precipitation commonly exceeding 100 mm (Fig. 2B). When hit by occasional typhoons, hourly intensities of precipitation can be above 100 mm. No clear correlation is found by visual comparison between the annual precipitation and the El Niño index (Fig. 2C) or the Western Pacific Monsoon index (Fig. 2D). The mean annual temperature difference is very large (~20°C) with severe snowfall from October to May. Because of these climatic and topographic conditions, physical weathering and soil loss are severe. Bedrock outcrops thus occupy the majority of the Seoraksan area. In the rest of the area, effective soil depth is only about 20 cm (Seoraksan National Park Service, 2008). Poor development of herbaceous plants on the soil, composed mainly of sandy loam, is also one of the important causes of severe soil loss. Mass wasting, dominated by rockfalls, and torrential streamflows have thus been regarded to be the main agents of geomorphic changes (Migoñ et al., 2019). No alluvial fan has been reported in the Seoraksan area before 2006, although old bajada-like pediment surfaces are found locally at mountain fronts outside the study area.

From July 9 to July 18, 2006, 671 mm of rainfall with hourly intensities over 100 mm was recorded in the Seorak-

san area. Although the total and the daily precipitations during this period were not particularly high compared with other years (Fig. 2B), the rainfall caused severe valley erosion in dozens of places in the national park. The valley erosion occurred as rainwater and eroded soil on the hillslope rushed down into the valleys. The streamflows uprooted trees and eroded bouldery rockfall debris on the valley floors, exposing the light-colored granitic bedrock along their paths (Fig. 1C). A conspicuous fan-shaped landform was produced at the exit of the Geoncheongol valley, where it joins the Hangyecheon stream. According to eyewitness accounts, which were obtained through direct interviews with local residents, the fan formed in the midnight of the heaviest rain, accompanied by rumbling noises. Comparison of aerial photographs suggests that the fan did not exist before 2006 (Fig. 3A). The fan is 170 m long and 330 m wide and has an area of 0.03 km². The catchment area of the fan is 2.0 km². The fan area is very small compared to the catchment area (cf. Kochel and Johnson, 1984) because of the limited space in which the fan could be made, bounded by the Hangyecheon stream. The area of exposed bedrock after the rainfall in the catchment area is 0.25 km². About 50,000 m³ of soil and an unmeasurable amount of rockfall debris on the valley floors are estimated to have been eroded by this rainfall-induced event. The slope of the fan surface is 6.8°, and the average slope of the main valley in the catchment area is 14°. The topographic analysis was made on 1:5,000 digital topographic maps, which were produced in 2017 by the National Geographic Information Institute of Korea (<https://www.ngii.go.kr/eng/main.do>).

DEPOSIT FEATURES

The sediments on the fan are divided into three facies based on grain size, depositional morphology, and relief: boulder mounds, cobble bars/sheets, and channels. Spatial distribution of the facies before 2020 was measured from aerial photographs. The facies distribution in 2020 was measured by field surveying and aerial photography using a drone in the spring and fall of that year. The boulder mounds occur from near the fan apex to the toe with a radially elongated shape in plan view (Fig. 3). They are a few tens of meters wide and over a hundred meters long, and composed of clast-supported and mostly openwork boulders with some sand matrix in the interior (Fig. 4A–D). They occupied about 42% of the fan area in 2008, but the area decreased to about 15% in 2020 (Fig. 3E–G). They have a positive relief of over 5 m relative to the surroundings with abrupt margins. The frontal and lateral margins are commonly steeply inclined (Fig. 4A–C), whereas the rear margins have less pronounced relief (Fig. 4D). Clast imbrication is indistinct because of the mostly blocky and equant form of the gravel clasts. Very crude and laterally impersistent stratification is locally recognized by subtle variations of clast sizes. Downfan variations in clast sizes are not obvious between proximal and distal localities.

The cobble bars/sheets occupy the majority of the fan surface (Fig. 4E). Comparison of aerial photographs shows

that their area has increased steadily since the fan formation (Fig. 3E–H). Their surface is incised by shallow channels that are less than a meter deep, radiate generally from the fan apex, and overall have a braided distributary channel pattern (Fig. 4E). They are composed mainly of clast-supported and commonly openwork cobbles with minor amounts of pebbles and boulders on the surface (Fig. 4C–D). However, their interiors, observable at a few eroded channel walls, contain medium to coarse sand matrix, and rarely show crude stratification with locally openwork gravel layers (Fig. 4G). Some cobble deposits show scaled-down morphology of boulder mounds, composed of large boulders at the front with the finer-grained and openwork gravels trapped behind them (Fig. 4F). Channels are a few meters deep and incised into the cobble bars/sheets (Fig. 4H), locally dissecting a nearby boulder mound (Fig. 4A). Large boulders, locally in excess of several meters in diameter, are scattered on the channel floors.

DEPOSITIONAL PROCESSES

The changing facies distribution on the fan (Fig. 3) suggests that the boulder mounds, shrinking in area year by year, were produced by the 2006 rainfall event, whereas the cobble bars/sheets and channels, which increase in area

and gradually cover the boulder mound area, were produced mostly by multiple rainfall events after 2006. Cobble bars/sheets of the 2006 event may be locally present on the surface, but are inferred to have been mostly buried, reworked, or eroded by post-2006 events.

The boulder mounds are interpreted to have formed by torrential sheetfloods, which possibly had the properties of hyperconcentrated flood flows temporarily. Their radially elongated shape and mound-like morphology is clearly distinguished from the deposit geometry of debris flows characterized by levees and lobes (Blair and McPherson, 1998) (Fig. 5). The overall lack of muddy to sandy matrix also negates the role of debris flow processes. The lack of matrix can possibly be due to post-depositional removal by recessional or later sheetfloods. Near absence of pebble- to cobble-size gravel in the interstices between boulder clasts (e.g., Fig. 4D) suggests, however, that the boulder mounds were initially made up of only boulders. Almost complete removal of pebble- to cobble-size gravel in the interstices of bouldery deposits together with muddy to sandy matrix by recessional or later sheetfloods is hardly conceivable. The sand matrix-filled interior of the boulder mound in Figure 4A suggests that both coarse and fine particles could be deposited together at an early stage of mound formation because the flood flow had a high particle concentration, similar to a hyperconcentrated flood flow. However, the flow changed promptly into a water flood, selectively depositing the boulder clasts in the mound and transporting the finer gravel clasts and the liquid component with suspended sand and mud further downfan. Such separation of a flow into solid and liquid components during deposition is an unlikely process in debris flows (Costa, 1988).

The boulder mounds are similar to the transitional-flow deposits of Wells and Harvey (1987) in that they have lobate geometry with steep margins, comprise matrix-free upper zones and matrix-rich lower zones, and show local crude stratification. The boulders are interpreted to have been transported as rolling and sliding bedload, and deposited rapidly as the sheetflood expanded and decelerated. The development of boulder jams that can cause local flow deceleration and flow separation around them might have led to the deposition of boulders (Blair, 1987). The boulders are inferred to have accumulated clast-by-clast in an upfan direction and then by avalanching of clasts on steeply inclined fronts and lateral margins of the mounds (Fig. 5B). The avalanching of clasts resulted in local concentrations of large clasts at the front and margin of the boulder mounds (Fig. 4A–B), which can be confused with megaclast concentrations at the front of a debris-flow lobe produced by frictional freezing of clasts pushed forward by the more fluid and mobile debris-flow body (Pierson, 1980, 1986) (Fig. 5A).

The cobble bars/sheets are also interpreted to have formed by sheetfloods (Wells and Harvey, 1987), which were generated by both 2006 and post-2006 rainfall events. Year-by-year increase of the area occupied by the cobble deposits (Fig. 3) suggest that the majority of the deposits

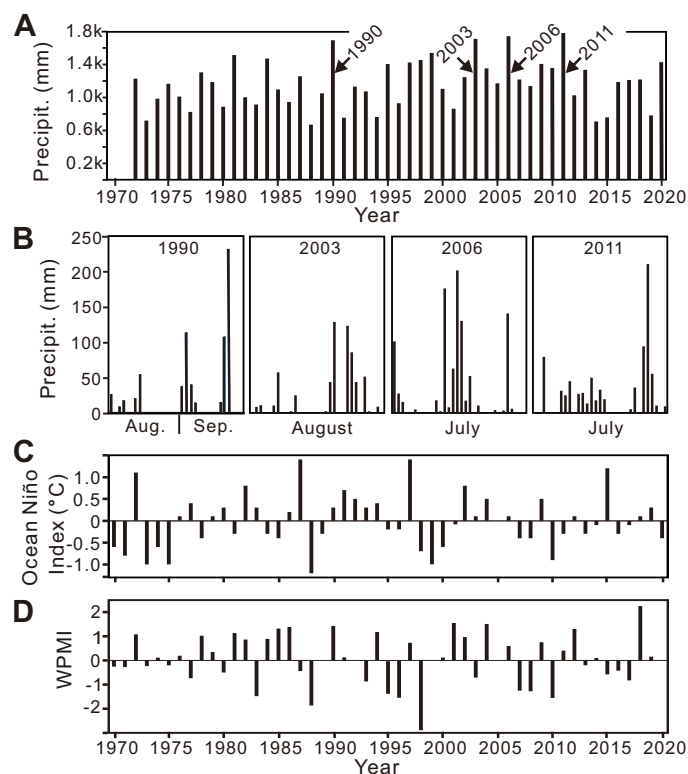


Figure 2: Meteorological data. **A:** Annual precipitation in Seoraksan since 1972 (data available at <http://www.weather.go.kr>). **B:** Daily precipitation during the months of the heaviest rainfall in 1990, 2003, 2006, and 2011. **C:** The Oceanic Niño Index since 1970 (data available at <http://origin.cpc.ncep.noaa.gov>). **D:** The Western Pacific Monsoon Index since 1970 (data available at <http://apdrc.soest.hawaii.edu>).

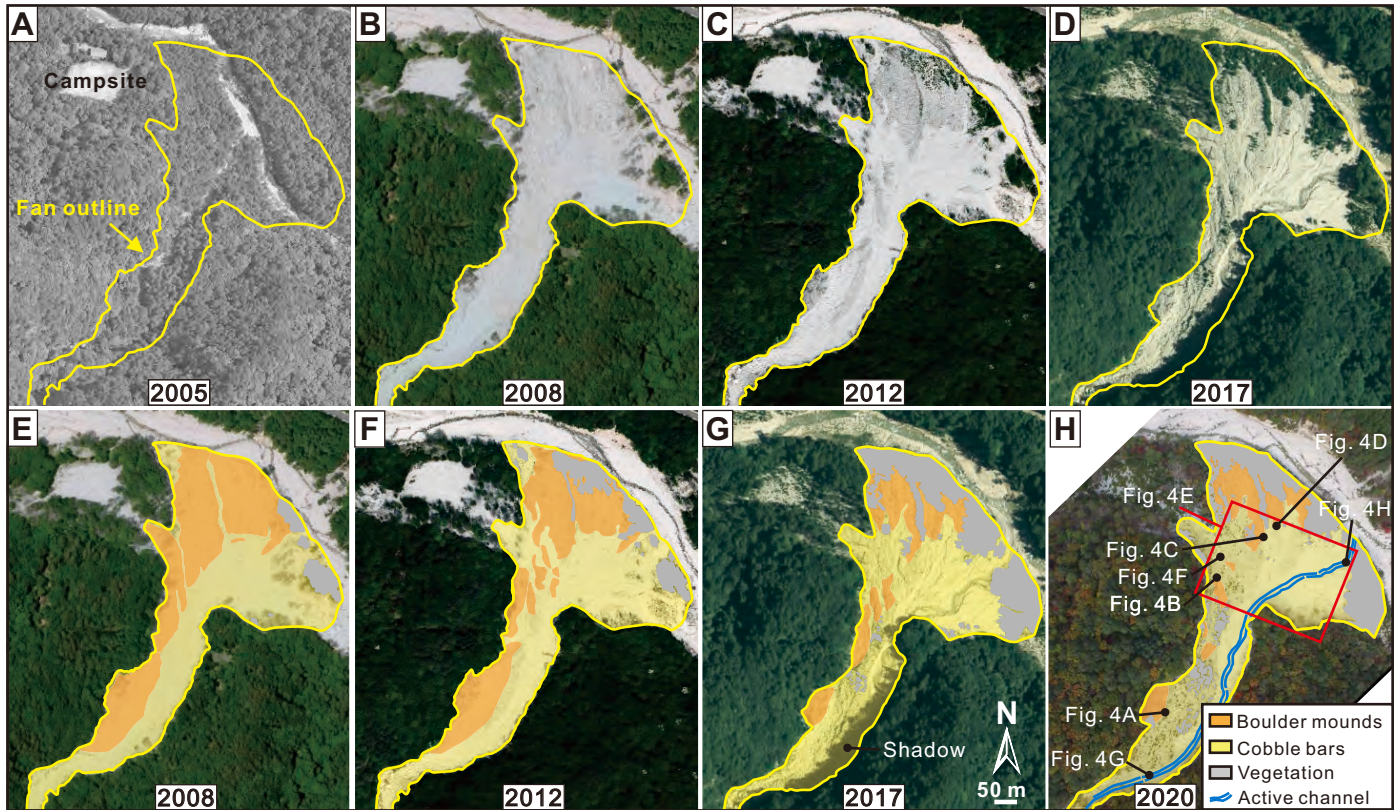


Figure 3: Changes of the fan surface. **A–D:** Aerial photographs taken between 2005 and 2017. **E–H:** Changes of sediment facies on the fan (Photograph A is available at <http://www.ngii.go.kr>, photographs B to G are available at <http://map.kakao.com>, and photograph H was taken with an unmanned aerial vehicle by the authors).

on the surface resulted from post-2006 sheetflood events, which probably eroded and reworked the 2006 deposits. The overall braided bar- and channel-like pattern of the deposits (Fig. 4E), some of them having the scaled-down morphology of the boulder mounds (e.g., Fig. 4F), suggest that they were also produced by the accumulation of gravelly bedload transported by sheetfloods followed by shallow incision of the deposits by recessional water flows. Scour marks on rare tree trunks standing upright (Fig. 4H) also suggest numerous collisions of gravel clasts carried as bedload in the floods. Crude stratification of the deposits with local intercalations of openwork gravel layers (Fig. 4G) suggests multiple depositional events by sheetfloods with intervening erosional or reworking and winnowing events. Almost complete removal of the trees on the fan surface by the 2006 event (Fig. 3B) suggests that the floods had competency that was high enough to knock down trees even at the fan toe. The significant change of the course of the Hangyecheon stream (Fig. 3A–B) is also notable, which is attributed to the encroachment of the bouldery fan into the former stream channel.

Stratigraphic arrangement of the boulder mounds, cobble bars/sheets, and channels is poorly constrained. Continual shrinking of the boulder mound area since 2006 (Fig. 3) suggests that these mounds were produced by the 2006 event only, whereas the ever-increasing area of the

cobble bars/sheets indicates their deposition mostly from multiple post-2006 events. Some cobble deposits are, however, apparently overlain by the frontal and lateral parts of the boulder mounds (Fig. 4B–C), suggesting that the formation of the boulder mounds was preceded by the deposition of cobble deposits during the 2006 event. We therefore interpret that the deposition of the boulder mounds occurred during the peak discharge, while the cobble bars/sheets were deposited both before and after the peak discharge during the 2006 rainfall event. It is uncertain whether the cobble deposits overlying the rear part of the boulder mounds (Fig. 4D) were produced by the 2006 event or the post-2006 events. Whatever the case, we interpret that the deposition of cobbles could occur both before and after the boulder mound formation, i.e., before and after the peak discharge.

The unusually high relief of the boulder mounds and the absence of pebble to cobble gravel in the interstices of the bouldery deposits (e.g., Fig. 4C–D) suggest that the boulder mounds were quickly exposed above floodwater after the peak discharge, and could not trap finer gravel clasts that were transported by the waning or recessional flood or by the post-2006 floods. Meter-deep channels with steep walls and scattered boulders on the floor (Fig. 4H) are interpreted to be erosional features produced by confined streamflows, which led to channel incision and drainage

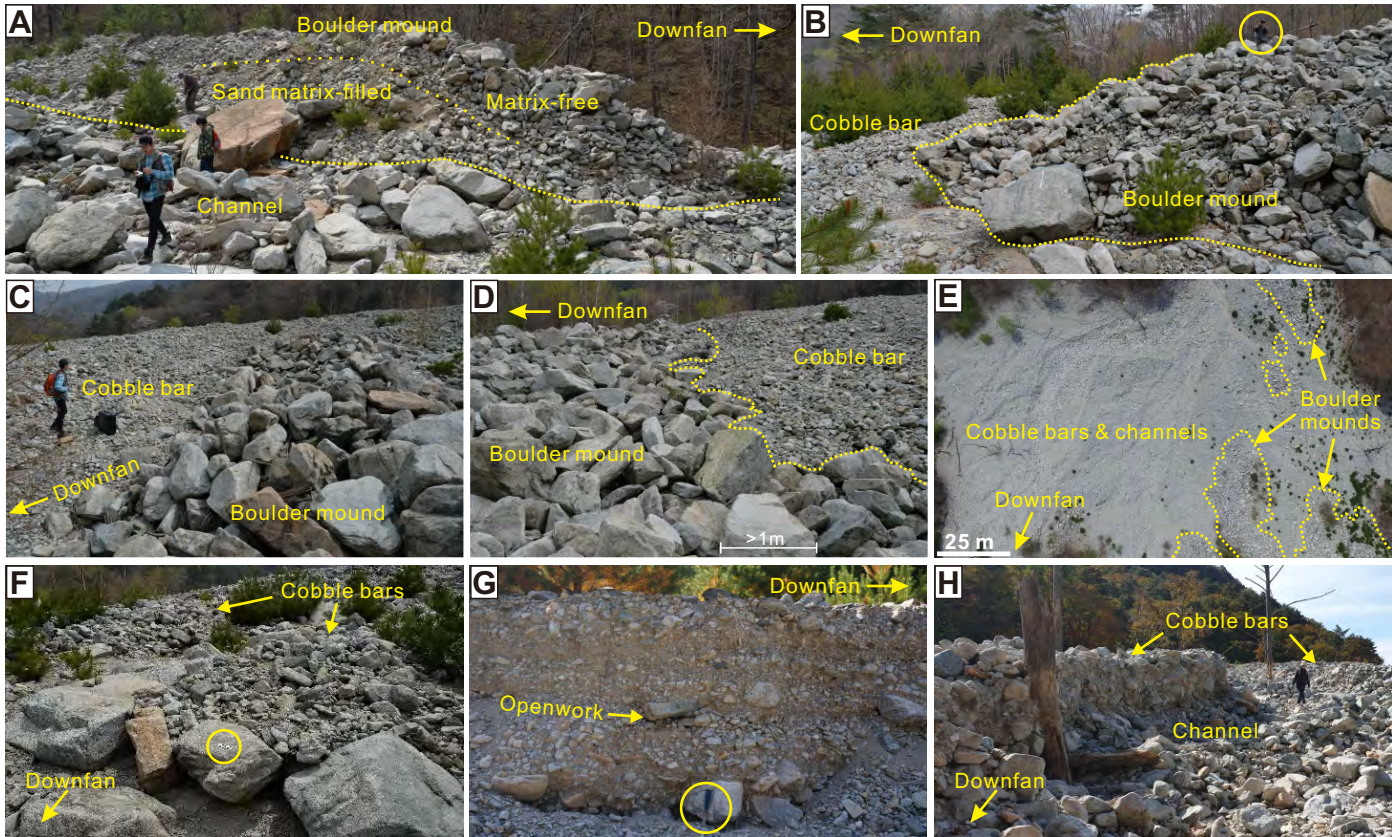


Figure 4: Deposit features. **A:** Longitudinal section of a boulder mound dissected by an abandoned channel in the foreground. **B:** Frontal margin of a boulder mound overlying cobble bar deposit. A figure (circled) gives the scale. **C:** Lateral margin of a boulder mound overlying cobble bar deposit. **D:** Rear margin of a boulder mound partly overlain by cobble bar deposit. **E:** Aerial photograph of the fan surface taken with a drone in 2020. **F:** A cobble bar with a frontal boulder jam. A 10 cm-long photo scale is circled. **G:** Crudely stratified, relatively fine-grained cobble bar deposit with medium to coarse sand matrix and an openwork gravel layer. A hammer (circled) for scale. **H:** An active channel incised into cobble bar deposits. Note the scour marks on the moribund tree trunks. The locations of the photographs are shown in Figure 3H.

network development on the fan surface over a decade. For example, the channel in Figure 4H was eroded by more than a meter after a typhoon-induced rainfall in 2020.

CONTROLS ON ALLUVIAL FAN FORMATION

Climate change and tectonic activity are the main extrinsic controls of alluvial fan formation that operate independently of an alluvial fan system. These two controls probably created the topographic and environmental conditions in the Seoraksan area over a long period of time setting up the conditions for an alluvial fan to be formed. However, the specific timing and location of the alluvial fan formation are not likely to have been determined by these two factors because no significant tectonism or seismicity has been reported in the study area recently, and the episodic fan formation in 2006, but not in 1990, 2003 or 2011 when the precipitation was similar (Fig. 2B), cannot be related to climate changes between these years.

On the other hand, intrinsic geomorphic processes in the source area combined with the role of the geomorphic threshold (Schumm, 1979) are interpreted to have triggered the episodic formation of the Seoraksan alluvial fan. Ac-

cording to the concept of the geomorphic threshold, the formation of the Seoraksan alluvial fan can be regarded as an episodic response of the source area to the stresses applied to that area over a length of time until a threshold is reached. The present catchment area of the alluvial fan is presumed to be near the stage of maximum drainage extension, characterized by tributary valley development to near the watershed (Fig. 1C). Slope erosion is inferred to be at or near its maximum with high production of coarse sediment. The trunk valley and its major tributary valleys might have been, however, reducing their ability to transport coarse sediment and increasing their storage capacity because of the tendency for stages of drainage basin evolution to overlap in time (Schumm, 1979). A threshold condition was probably reached as coarse sediments aggraded valley floors to the point of metastability. A heavy rainfall event in 2006, which would have had no extreme effects before the valleys were substantially aggraded, might have triggered massive remobilization of bouldery sediments on the valley floors and the formation of the bouldery alluvial fan.

Afterwards, only the modification of the fan surface oc-

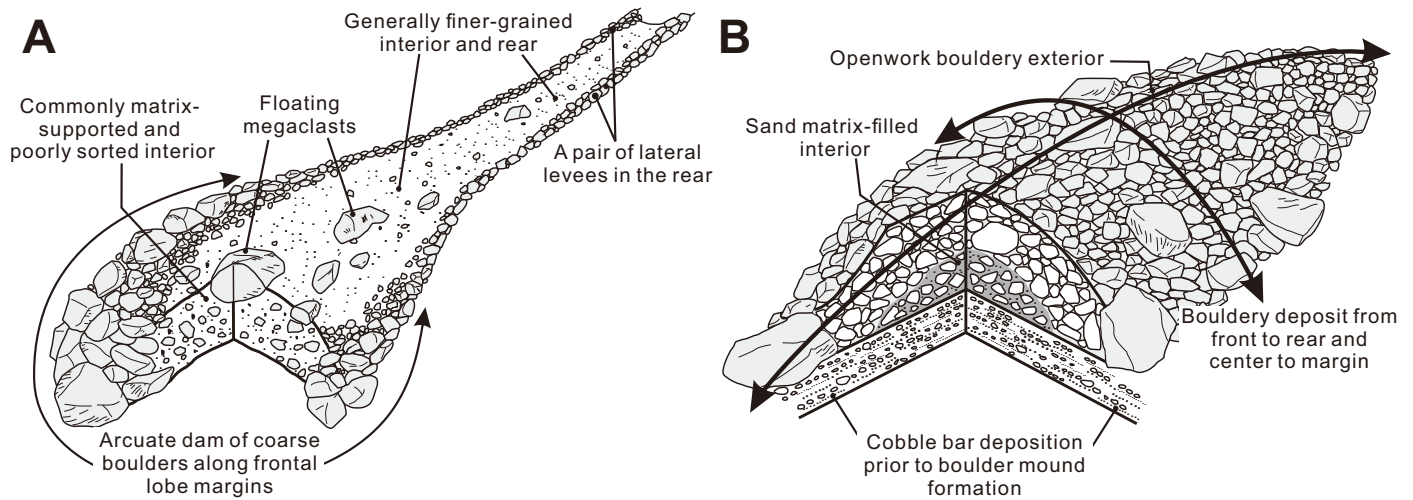


Figure 5: Comparison of debris-flow lobe/levees and boulder mounds of Seoraksan. **A:** Debris flow deposits are characterized by an arcuate dam of boulders along the lobe margins and by parallel levees in the rear. Their interior is composed of commonly matrix-supported and poorly sorted deposits with floating megaclasts (Pierson, 1980, 1986, Blair and McPherson, 1998). **B:** The boulder mounds of Seoraksan are, however, covered by openwork boulders on the entire surface from front to rear and from center to margin. The cobble bar deposit at the base is interpreted to be deposited by sheetfloods before the peak discharge; the sand matrix-filled interior is by hyperconcentrated flood flows; the openwork bouldery exterior is by torrential water flood during the peak discharge. The boulder mounds are up to 5 m high, tens of meters wide, and over a few hundreds of meters long. Debris flow lobe/levees also have similar dimensions.

curred in spite of a few intense rainfall events after 2006 (Fig. 2A–B), probably because the threshold condition was removed in the catchment area. The Seoraksan alluvial fan thus demonstrates that alluvial fans in humid-temperate regions, which have been considered to form by relatively slower and continuous processes, can form in an instant in time, and that the instantaneous fan formation can be triggered by a single, casual hydro-meteorological event if intrinsic geomorphic threshold conditions are met in the source area. The Seoraksan alluvial fan thus highlights the role of geomorphic threshold in causing drastic changes in the hydrologic performance of the watershed.

CONCLUSIONS

Alluvial fans are a type of distributive fluvial system (DFS), which is defined as ‘the deposit of a fluvial system which in planform displays a radial distributive channel pattern’ (Hartley et al., 2010). Some workers claim that the term ‘alluvial fan’ is no longer necessary and can be replaced with the term DFS or ‘small DFS’ because the DFS display the characteristics of alluvial fans at all scales (Weissmann et al., 2010, 2015). However, the term alluvial fan has been widely used for a long time in earth science communities, entrenched in the literature, and appears to be still useful for describing conical, commonly coarse-grained sedimentary bodies formed at the mouths of mountain valleys or in a piedmont setting and for distinguishing them from rivers or river deltas (Blair and McPherson, 1994), even if there is a continuum between fans and rivers.

The Melton ratio, defined as watershed relief divided by the square root of watershed area (Melton, 1957), of the Seoraksan alluvial fan is 0.7, and the watershed length

is 2.4 km. According to these watershed morphometrics, the watershed of the Seoraksan alluvial fan is predicted to be prone to debris flows (Wilford et al., 2004). The main depositional processes on the fan are, however, interpreted to be water floods and hyperconcentrated flood flows. The discrepancy between the predicted and the actual depositional processes resulted most likely from the lack of soils on the hillslopes and fine-grained sediments on the valley floors in Seoraksan that could form the matrix of debris flows. This indicates that the use only of topographic factors, without the consideration of field-based datasets, can lead to wrong prediction of hazards in mountainous areas. Defining and interpreting the alluvial fan types and the dominant hydrogeomorphic processes based solely on topographic factors, which are being conducted in some academic circles, can also lead to serious misinterpretation of the nature of alluvial fans.

The Seoraksan alluvial fan is distinguished from either arid-region or humid-region alluvial fans and either debris flow-dominated or streamflow-dominated alluvial fans in that

1. the fan was produced by a single seasonal rainfall, which was not necessarily of a very rare and unusually intense event,
2. the main depositional processes were sheetfloods or hyperconcentrated flood flows, rather than debris flows or constant to seasonal braided streamflows,
3. the deposits are unusually coarse-grained and devoid of mud or muddy sand matrix and fine-grained over-

bank facies, dissimilar to either debris-flow or stream-flow deposits, and

4. the streamflows acted mainly as erosional rather than depositional processes after the fan formation (cf. Kochel and Johnson, 1984, Evans, 1991, Nemeč and Postma, 1993).

The Seoraksan alluvial fan can more likely be described as a 'sheetflood-dominated alluvial fan', which has long been documented in the literature (e.g., Blair, 1987, Wells and Harvey, 1987, among others) but has largely been ignored or misrepresented in the scientific communities (Blair and McPherson, 1994). The Seoraksan alluvial fan can thus serve to develop sedimentological models for sheetflood-dominated alluvial fans, which are presumed to occur in abundance and in diverse forms in glacial to periglacial, tropical, and temperate environments.

ACKNOWLEDGMENTS

This research was funded by the projects for the potential nomination of Mt. Seoraksan on UNESCO World Heritage List, which were supported by the Inje County, Gangwon Province, and the Cultural Heritage Administration of Korea.

Literature Cited

- Blair, T. C. (1987). Sedimentary processes, vertical stratification sequences, and geomorphology of the Roaring River alluvial fan, Rocky Mountain National Park, Colorado. *Journal of Sedimentary Research*, 57(1):1–18.
- Blair, T. C. and McPherson, J. G. (1994). Alluvial fans and their natural distinction from rivers based on morphology, hydraulic processes, sedimentary processes, and facies assemblages. *Journal of Sedimentary Research*, 64(3a):450–489.
- Blair, T. C. and McPherson, J. G. (1998). Recent debris-flow processes and resultant form and facies of the Dolomite alluvial fan, Owens Valley, California. *Journal of Sedimentary Research*, 68(5):800–818.
- Bull, W. B. (1977). The alluvial-fan environment. *Progress in Physical Geography*, 1(2):222–270.
- Cabr e, A., Remy, D., Aguilar, G., Carretier, S., and Riquelme, R. (2020). Mapping rainstorm erosion associated with an individual storm from InSAR coherence loss validated by field evidence for the Atacama Desert. *Earth Surface Processes and Landforms*, 45(9):2091–2106.
- Cho, D. L. (1994). Hornblende geobarometry of the Mesozoic granitoids in South Korea and the evolution of the crustal thickness. *Journal of the Geological Society of Korea*, 30:41–61.
- Costa, J. E. (1988). Rheologic, geomorphic and sedimentologic differentiation of water floods, hyperconcentrated flows and debris flows. In Baker, V. R., Kochel, R. C., and Patton, P. C., editors, *Flood Geomorphology*, pages 113–122. Wiley-Intersciences Publications.
- Evans, J. E. (1991). Facies relationships, alluvial architecture, and paleohydrology of a Paleogene, humid-tropical alluvial-fan system; Chumstick Formation, Washington State, USA. *Journal of Sedimentary Research*, 61(5):732–755.
- Hartley, A. J., Weissmann, G. S., Nichols, G. J., and Warwick, G. L. (2010). Large distributive fluvial systems: characteristics, distribution, and controls on development. *Journal of Sedimentary Research*, 80(2):167–183.
- Harvey, A. M. (2007). Differential recovery from the effects of a 100-year storm: Significance of long-term hillslope–channel coupling; Howgill Fells, northwest England. *Geomorphology*, 84(3–4):192–208.
- Kee, W. S., Kim, H., Kim, B. C., Choi, S. J., Park, S. I., and Hwang, S. K. (2010). Geological Report of the Seoraksan Sheet. Scale 1: 50,000. *Korea Institute of Geoscience and Mineral Resources*.
- Kochel, R. C. and Johnson, R. A. (1984). Geomorphology and sedimentology of humid-temperate alluvial fans, central Virginia. In Koster, E. H. and Steel, R. J., editors, *Sedimentology of Gravels and Conglomerates*, Memoir 10, pages 109–122. Canadian Society of Petroleum Geologists.
- LaHusen, S. R., Duvall, A. R., Booth, A. M., Grant, A., Mishkin, B. A., Montgomery, D. R., Struble, W., Roering, J. J., and Wartman, J. (2020). Rainfall triggers more deep-seated landslides than Cascadia earthquakes in the Oregon Coast Range, USA. *Science Advances*, 6(38):eaba6790.
- Marchi, L., Cavalli, M., Sangati, M., and Borga, M. (2009). Hydrometeorological controls and erosive response of an extreme alpine debris flow. *Hydrological Processes: An International Journal*, 23(19):2714–2727.
- McDonald, E. V., McFadden, L. D., and Wells, S. G. (2003). Regional response of alluvial fans to the Pleistocene-Holocene climatic transition, Mojave Desert, California. In Enzel, Y., Wells, S., and Lancaster, N., editors, *Paleoenvironments and Paleohydrology of the Mojave and Southern Great Basin Deserts*, Special Paper 368, pages 189–206, Geological Society of America.
- Melton, M. A. (1957). An analysis of the relations among elements of climate, surface properties, and geomorphology. Technical report, Columbia University, New York.
- Migoñ, P., Kasprzak, M., and Woo, K. S. (2019). Granite Landform Diversity and Dynamics Underpin Geoheritage Values of Seoraksan Mountains, Republic of Korea. *Geoheritage*, 11(3):751–764.
- Nemeč, W. and Postma, G. (1993). Quaternary alluvial fans in southwestern Crete: sedimentation processes and geomorphic evolution. In Marzo, M. and Puigdef abregas, C., editors, *Alluvial Sedimentation*, Special Publication 17, pages 235–276. International Association of Sedimentologists.
- Pierson, T. C. (1980). Erosion and deposition by debris flows at Mt Thomas, north Canterbury, New Zealand. *Earth Surface Processes*, 5(3):227–247.
- Pierson, T. C. (1986). Flow behavior of channelized debris flows Mount St. Helens Washington. In Abrahams, A. D., editor, *Hillslope Processes*, pages 269–296. Boston, Allen & Unwin.
- Schumm, S. A. (1979). Geomorphic thresholds: the concept and its applications. *Transactions of the Institute of British Geographers*, 4(4):485–515.
- Seoraksan National Park Service (2008). Monitoring of resources in Seoraksan National Park. Technical report, Sokcho.
- Weissmann, G. S., Hartley, A. J., Nichols, G. J., Scuderi, L. A., Olson, M., Buehler, H., and Banteah, R. (2010). Fluvial form in modern continental sedimentary basins: distributive fluvial systems. *Geology*, 38(1):39–42.
- Weissmann, G. S., Hartley, A. J., Scuderi, L. A., Nichols, G. J., Owen, A., Wright, S., Felicia, A. L., Holland, F., and Anaya, F. M. L. (2015). Fluvial geomorphic elements in modern sedimentary basins and their potential preservation in the rock record: a review. *Geomorphology*, 250:187–219.
- Wells, S. G. and Harvey, A. M. (1987). Sedimentologic and geomorphic variations in storm-generated alluvial fans, Howgill Fells, northwest England. *Geological Society of America Bulletin*, 98(2):182–198.
- Wilford, D. J., Sakals, M. E., Innes, J. L., Sidle, R. C., and Bergerud, W. A. (2004). Recognition of debris flow, debris flood and flood hazard through watershed morphometrics. *Landslides*, 1(1):61–66.

Identifying elusive piercing points along the North American transform margin using mixture modeling of detrital zircon data from sedimentary units and their crystalline sources

J. Clark Gilbert^{1,*}, Zane R. Jobe¹, Samuel A. Johnstone² and Glenn R. Sharman³

¹Department of Geology and Geological Engineering, Colorado School of Mines, Golden, CO 80401 USA

²U.S. Geological Survey, Geosciences and Environmental Change Science Center, Denver, CO 80225 USA

³Department of Geosciences, University of Arkansas, Fayetteville, AR 72701 USA

ABSTRACT The San Gabriel and Canton faults represent early stages in the development of the San Andreas fault system. However, questions of timing of initiation and magnitude of slip on these structures remain unresolved, with published estimates ranging from 42–75 km and likely starting in the Miocene. This uncertainty in slip history reflects an absence of appropriate piercing points. We attempt to better constrain the slip history on these faults by quantifying the changing proportions of source terranes contributing sediment to the Ventura Basin, California, through the Cenozoic, including refining data for a key piercing point.

Ventura Basin sediments show an increase in detrital zircon U-Pb dates and mineral abundances associated with crystalline sources in the northern San Gabriel Mountains through time, which we interpret to record the basin's northwest translation by dextral strike-slip faulting. In particular, an Oligocene unit mapped as part of the extra-regional Sespe Formation instead has greater affinity to the Vasquez Formation. Specifically, the presence of a unimodal population of ~1180 Ma zircon, high (57%) plagioclase content, and proximal alluvial fan facies indicate that the basin was adjacent to the San Gabriel anorthosite during deposition of the Vasquez Formation, requiring 35–60 km of slip on the San Gabriel-Canton fault system. Mixture modeling of detrital zircon data supported by automated mineralogy highlights the importance of this piercing point along the San Gabriel-Canton fault system and suggests that fault slip began during the late Oligocene to early Miocene, which is earlier than published models. These two lines of evidence disagree with recent models that estimate >60 km of offset, requiring a reappraisal of the slip history of an early strand of the San Andreas transform zone.

KEYWORDS detrital zircon geochronology, strike-slip tectonics, tectonic reconstruction, tectonostratigraphy

INTRODUCTION AND TECTONIC HISTORY

The San Andreas Fault is currently the primary geologic boundary between the Pacific and North American plates. This plate boundary is the most studied in the world due to its complex change from a convergent to transform margin beginning at ~28 Ma (Atwater, 1989) and its inherent seismicity and proximity to large population centers. The San Gabriel and Canton faults are older strands of the San Andreas fault system and despite decades of debate, existing reconstructions of slip are still in conflict. The two faults are herein considered the San Gabriel-Canton fault system (SGCF) due to their similar trend and offsetting basement features (Fig. 1).

Along transform margins, piercing points are interpreted

where similar basement features or contacts between sedimentary units intersect the fault trace (Crowell, 1962). Piercing points are useful references for structural restorations because many of these points were originally adjacent before later offset by lateral fault movement. However, slip offset and fault timing estimates often have high degrees of uncertainty. This is especially true when using sedimentary rocks because sediment routing is complex and dynamic near transform faults, and the paleogeography was likely different than it is today. Previous studies have utilized detrital zircon geochronology to restore piercing points along the North American transform margin (Sharman et al., 2013; Gooley et al., 2020). Past reconstructions of the SGCF recognized similarities between crystalline units in the San Gabriel Mountains (SGM) and at Frazier Mountain (Fig. 1), but disagreed on the magnitude of slip required to restore these piercing points to their pre-offset locations (~42–46 km, Powell, 1993; 60–75 km, Crowell, 2003). These models agreed that movement along the SGCF ended ~5

Copyright © 2021 by the Author(s)

doi: 10.2110/sedred.2021.2.3

Manuscript submitted: 02/19/2021

Received in revised format: 05/26/2021

Manuscript accepted: 06/03/2021

*Corresponding author: jclarkgilbert@gmail.com

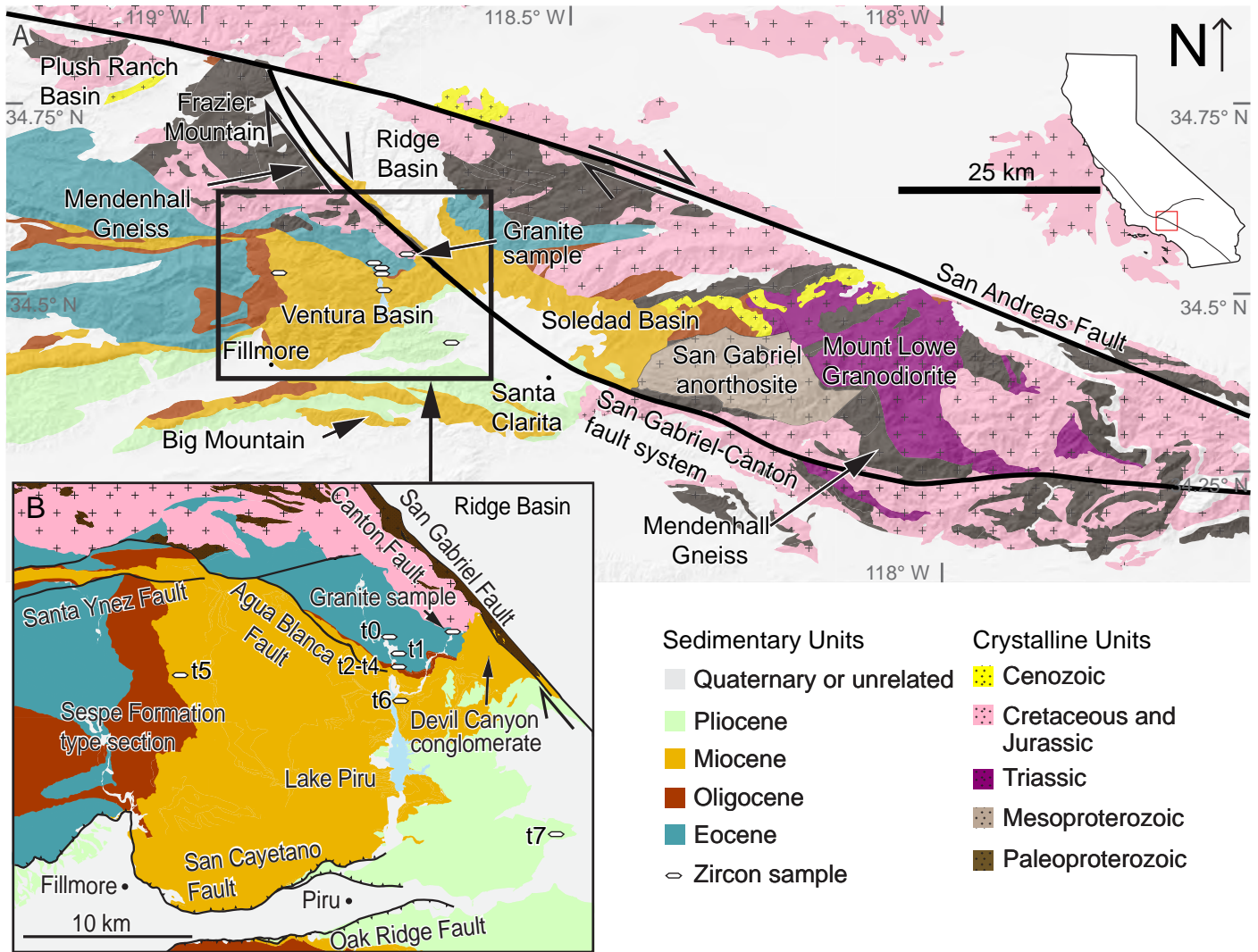


Figure 1: A) Geologic map of the eastern Ventura Basin (after Dibblee, 2010; Jennings, 2010; Jacobson et al., 2011). B) Inset map of the eastern Ventura Basin, showing sample locations t0-t7.

Ma when slip was transferred to the modern trace of the San Andreas Fault (Crowell, 1982; Powell, 1993). However, the early history of the SGCF remains unclear, and two models use the offset of the Mint Canyon Formation in the Soledad Basin to estimate a different timing of fault initiation (15–13 Ma, Powell, 1993; ~18 Ma, Hoyt et al., 2018).

Sedimentary units within the Ventura Basin record deposition adjacent to the SGCF before, during, and after SGCF slip (Fig. 1A; Yeats et al., 1994). Prior to SGCF initiation, Eocene marine sediments of the Juncal and Matilija Formations were deposited in a large, integrated catchment within the forearc basin created by the subduction of the Farallon Plate (Jacobson et al., 2011; Sharman et al., 2015). By Oligocene time, the forearc basin was filling with fluvial deposits of the Sespe Formation south of the study area (Ingersoll et al., 2018). In the study area, the clast size and mineralogy of Oligocene conglomerates suggests local sources in the emergent SGM and subsequent right-lateral

translation ~60 km (Bohannon, 1975) during the Miocene. Miocene deep-marine deposits of the Modelo Formation continued to record proximal sedimentation from the SGM (Rumelhart and Ingersoll, 1997). This pattern continued until Pliocene time, when the SGCF became inactive (Crowell, 2003).

Past reconstructions of slip along the SGCF used conglomerate clasts and multiple crystalline sources as piercing points, and provenance changes were interpreted as evidence of basin translation along the fault (Crowell, 1954; Bohannon, 1975). However, the heterogeneous mineralogy of these large clasts creates high uncertainty in previous total slip offset estimates; a more detailed and complete record of the provenance of the sand-sized fraction has not been completed. This study highlights an Oligocene sample with a unimodal age fraction that is a more appropriate indicator of provenance than sedimentary units used in previous reconstructions and documents continual changes in detrital zircon (DZ) age spectra and SEM-based

automated mineralogy (SAM) data in the Eocene-Pliocene Ventura Basin. We interpret this progression as a change in provenance as the basin translated northward along the SGCF. We demonstrate 35–60 km of slip on the SGCF likely initiating in Oligocene time and discuss the possible pre-Miocene slip history and the implications for the tectonic reconstruction of southern California.

METHODS

Eight samples were collected from the following units near Lake Piru, California, and numbered according to age (Fig 1B; Fig. 2): Eocene Juncal Formation (t0) and Matilija Formation (t1), Oligocene Vasquez Formation (t2, t3), Miocene Vaqueros Formation (t4) and Modelo Formation (t5, t6), and Pliocene Pico Formation (t7). Thin sections

were made for seven samples and analyzed with a Tescan Integrated Mineral Analyzer for SAM (Sylvester, 2012); sample t7 was not sufficiently lithified. Each sample was analyzed for the U-Pb dates of 120–150 zircon grains via LA-ICP-MS (Hart et al., 2016) at the University of Arkansas Trace Element and Radiogenic Isotope Laboratory.

Although we recognize that Eocene sediments are unlikely to be locally sourced (Jacobson et al., 2011; Sharman et al., 2015) and that some of these age components are not unique to the SGM, we assume that DZ of Oligocene-Pliocene samples were derived from four crystalline parent source components located in the modern SGM: Cretaceous-Jurassic granitoids (CJ) (200–26 Ma), the Triassic Mount Lowe Granodiorite (LG) (280–200 Ma), the Triassic Mount Lowe Granodiorite (LG) (280–200 Ma), the Mesoproterozoic San Gabriel anorthosite (SGA) (1300–1000

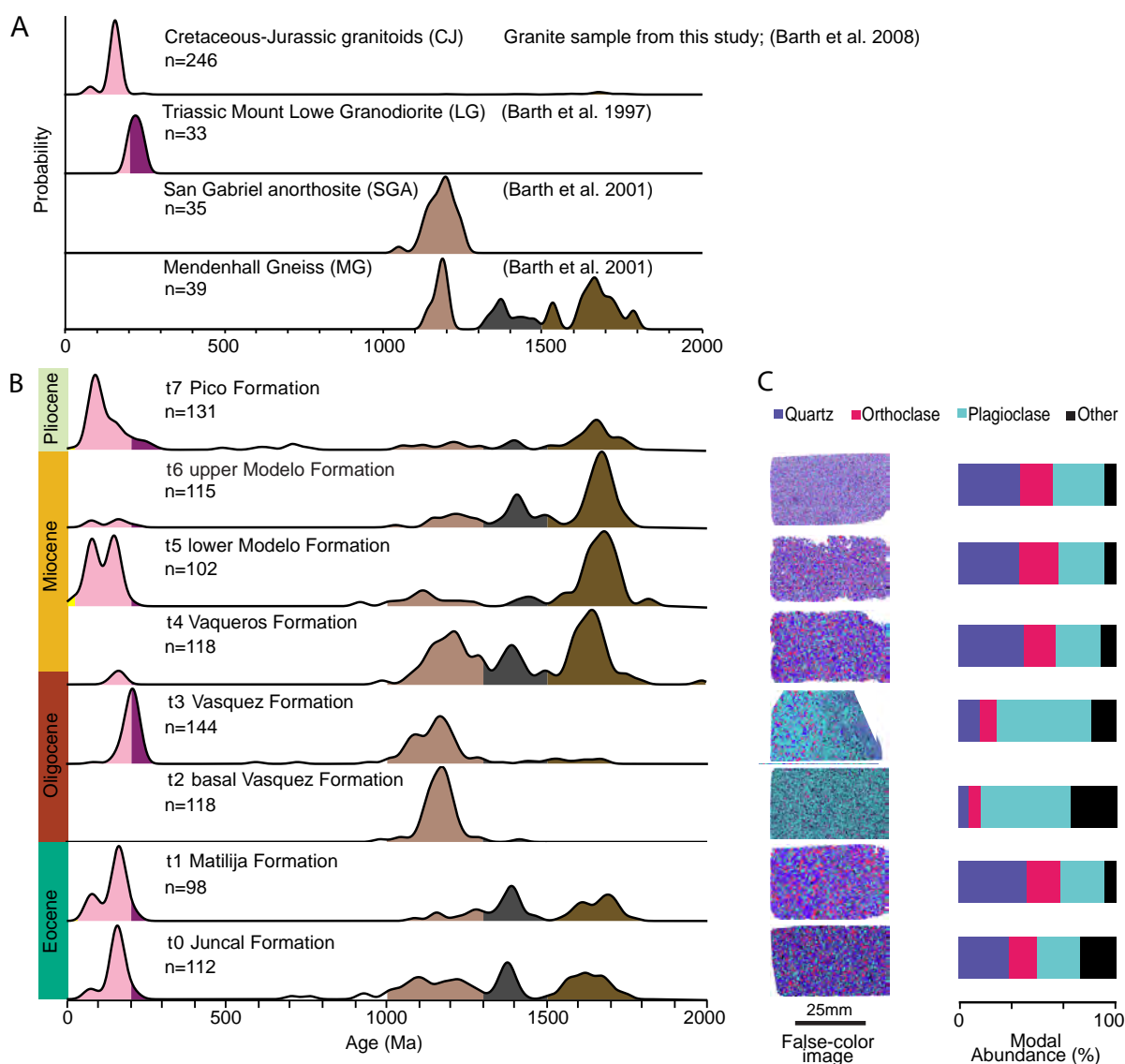


Figure 2: A) KDEs of zircon U-Pb dates from crystalline sources (parents). B) KDEs of DZ from eight Eocene-Pliocene samples (children). KDEs are not normalized and are constructed using a Gaussian kernel with a bandwidth of 20 Ma. C) Thin section false-color images of SAM data with abundant minerals labeled and bars plotting their modal abundances. The SAM and DZ data were analyzed from the same set of samples, but sample t7 was too disaggregated to make a thin section.

Ma), and the Paleoproterozoic Mendenhall Gneiss (MG) (multiple age peaks between 2000–1300 Ma). A granite sample (Fig. 1) was analyzed ($n=30$) and combined with published dates as the CJ parent, and the three other parents were compiled from published data (Fig. 2, Table S2). Although some formations may contain zircon recycled from older sedimentary units, we assume that recycled contributions were minor because each sample has a relatively unique age spectrum.

The contribution of each parent (crystalline source) was modeled for each child (detrital sample) following the ‘top-down’ approach of [Sharman and Johnstone \(2017\)](#). We characterized uncertainty in the mixture models using a bootstrapping approach ([Malkowski et al., 2019](#)). For each of 10,000 iterations, we resample with replacement the zircon dates from both the parent and child, calculate new kernel density estimates (KDEs), and determine the proportions of parents that mix to produce a distribution most similar to the resampled child distribution that is quantified with the Vmax metric (e.g., [Saylor and Sundell, 2016](#)). Detailed methods and data sources are included ([Supplemental Material, Tables S1–S5](#)).

RESULTS

Samples t0, t1, t4, t5, t6 and t7 contain 32–43% quartz, 17–29% orthoclase, and 25–33% plagioclase (Fig. 2B, Table S4). In contrast, the two Vasquez Formation samples (t2, t3) contain abundant plagioclase (t2, 57%; t3, 60%) and sparse quartz (t2, 6%; t3, 13%; Fig. 2B).

Eocene samples (t0–t1) contain abundant 200–26 Ma DZ and minor Permian-Triassic (280–200 Ma) and Proterozoic DZ (Fig. 2). Oligocene sample t2 contains a unimodal age fraction (1300–1000 Ma) while sample t3 has an approximately bimodal distribution consisting of older grains between 1300–1000 Ma and Phanerozoic grains between 250–140 Ma (upper Paleozoic and Mesozoic). Miocene sample t4 contains abundant 1300–1000 Ma and 2000–1500 Ma grains, samples (t5, t6) have variable Mesozoic and Proterozoic dates, and t5 has two Oligocene DZ dates. Pliocene sample t7 has DZ age modes between 200–26 Ma and 2000–1500 Ma.

Detrital zircon mixture modeling

Mixture models from Eocene samples (t0, t1) show consistent contributions from the MG (Fig. 3, Table S3; $P50=55-63\%$, $P2.5=26-45\%$, $P97.5=76-79\%$, where $P50$ is the median value and $P2.5$ and $P97.5$ are bounds on the 95% confidence interval); CJ forms a secondary source (Fig. 3). Mixture models for the Vasquez Formation samples (t2, t3) indicate strong contributions from the SGA ($P50=94-49\%$, $P2.5=81-29\%$, $P97.5=100-58\%$), with LG as a secondary source for t3 ($P50=37\%$, $P2.5=28\%$, $P97.5=47\%$). Models for samples from the Vaqueros (t4), Modelo (t5, t6), and Pico (t7) Formations all indicate MG to be the dominant source ($P50=55-100\%$, $P2.5=55-89\%$, $P97.5=87-100\%$), with SGA as a secondary source for t4 and CJ as a secondary source for t5, t6, and t7 (Fig. 3). SGA is not modeled to contribute

appreciable sediment to t5, t6, and t7.

DISCUSSION

Pre-Miocene deposition

The two lower Eocene samples (t0, t1) have similar DZ age spectra, with modeled contributions from MG and CJ sources currently exposed in the western SGM 60–80 km to the southeast (Figs. 1, 3). However, sources of this age are common in California and not spatially distinct (Fig. 1), and we interpret this mixture to represent deposition in the forearc basin from multiple, extra-regional sources.

Units containing samples t2 and t3 are mapped as the Sespe Formation ([Dibblee, 2010](#)), but these units are texturally immature, consisting of poorly sorted sandstones and conglomerates containing angular clasts up to 7 m ([Crowell, 1954](#); [Bohannon, 1975](#)), while the Sespe Formation is typically fine-grained, quartz-rich fluvial-deltaic deposits ([Ingersoll et al., 2018](#)). Instead, units t2 and t3 are more similar to the Miocene-Oligocene Vasquez Formation in the nearby Soledad Basin (Fig. 1A) ([Hendrix and Ingersoll, 1987](#)), and we suggest that units t2 and t3 represent locally sourced alluvial-fan deposits of the Vasquez Formation. This distinction is critical because while the age of the Sespe Formation is late Eocene–early Miocene ([Ingersoll et al., 2018](#)), the age of the Vasquez Formation is more tightly constrained between 25 and 21 Ma ([Hendrix and Ingersoll, 1987](#); [Frizzell Jr and Weigand, 1993](#)), which narrows the age uncertainty for a unit commonly used in tectonic reconstructions.

Previous models associated large clasts of anorthosite, granite, and gneiss in Eocene–Oligocene alluvial units to sources 60–75 km away in the SGA, LG, and MG, respectively ([Crowell, 1954](#); [Bohannon, 1975](#)). However, our DZ data sampled 4 km to the west of those outcrops favor a more spatially limited sediment source, because zircon dates that make up the ca. 1.2 Ga component in samples t2 and t3 are similar to the estimated age (1194 ± 35 Ma) of the SGA ([Barth et al., 2001](#)) (Fig. 1A). Furthermore, the abundant plagioclase (57–60%) and minor quartz (6–13%) in samples t2 and t3 (Fig. 2C) suggest a source rich in plagioclase, typical of anorthosites. These two lines of evidence suggest that, during Oligocene time, the Ventura Basin was 35–60 km to the southeast, where the SGA is nearest to the San Gabriel fault (Fig. 1). This location only requires an alluvial fan with a radius of 10–20 km to source the Vasquez Formation (t2 and t3), which is within the typical range (10–15 km) of alluvial fan radii ([Hartley et al., 2010](#)).

It is unclear why the sand-sized fraction is sourced only from the SGA (Fig. 2), while the boulder-sized fraction nearby is recording contributions from multiple sources ([Powell, 1993](#); [Crowell, 2003](#)). Several possible combinations of fault initiation timing, local paleogeography and grain size fractionation could contribute to this difference. Our preferred interpretation is that an alluvial fan emanating from the SGA carried the sand fraction to the south or west and into the study area, while another alluvial fan emanating from south of the SGA transported the boulders

to the north.

Miocene and Pliocene strike-slip associated sedimentation

DZ dates between 1300–1000 Ma diminish throughout Miocene time (Fig. 2); for example, a SGA contribution of 23% for t4 decreases to 0% for all younger samples (Fig. 3).

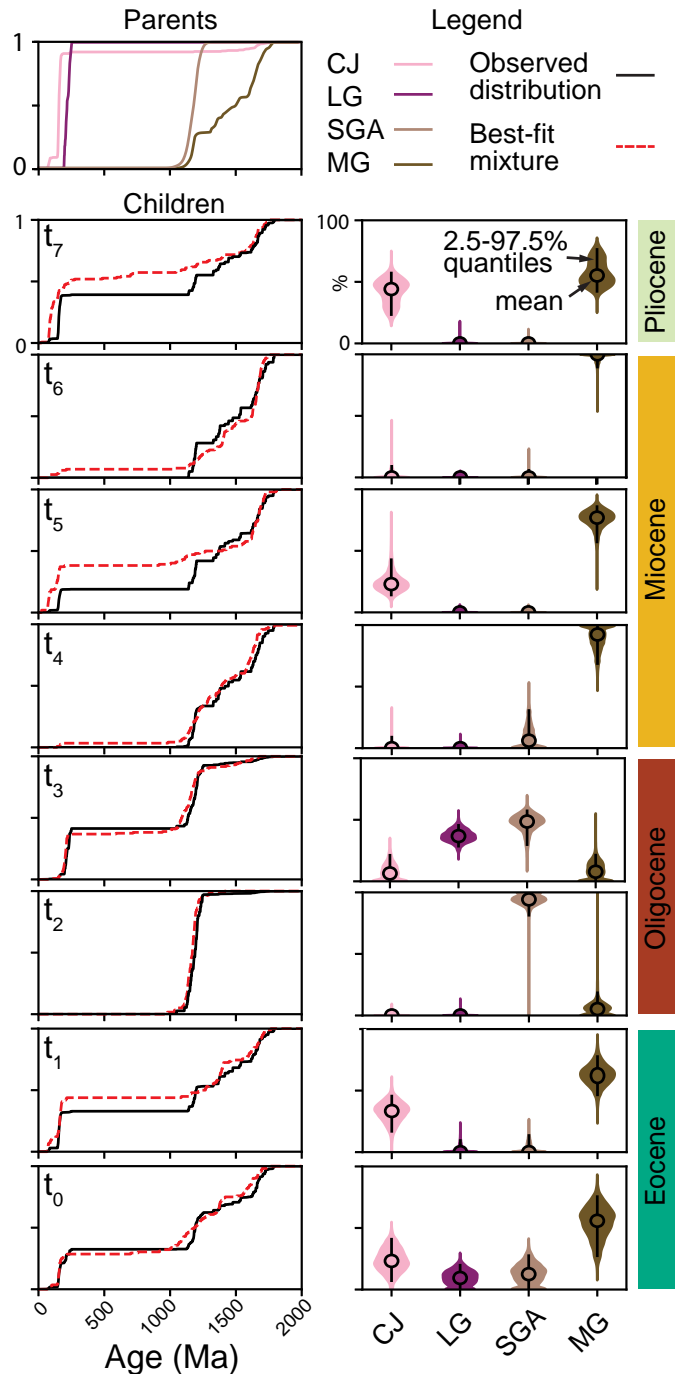


Figure 3: Left) Plots showing best-fit mixture-model results for each child sample using the Vmax comparison metric and the observed distribution. Right) Violin plots displaying range of uncertainty for each parent contribution from the resampling results.

We interpret this decrease to record the translation of the basin away from the SGA (Fig. 4). All of the best-fit mixtures from Miocene-Pliocene samples include significant but temporally variable input from MG, LG, and CJ (Fig. 2). We interpret these DZ components to represent deposition from the various sources exposed around the margins of the Soledad Basin (Fig. 1). MG and CJ rocks exist on the west side of the SGCF and technically could have provided sediment to the Ventura Basin during the Neogene. However, the occurrence of two Oligocene DZ dates analyzed in t5, likely sourced from volcanic units in the eastern Soledad Basin (Fig. 1), supports this provenance interpretation. We interpret the low proportions of >1 Ga zircon and strong CJ contribution in sample t7 as evidence of recycling of older sediments during Pliocene transpression and uplift (Ingersoll and Rumelhart, 1999; Crowell, 2003).

Explanation of piercing points and their uncertainties in the Ventura Basin

Figure 4B is a fault slip offset diagram of the relevant published reconstructions in which the boxes represent the uncertainty in the piercing points used to support the interpretations. The horizontal length of a given box represents the spatial uncertainty attributed to that piercing point, and the vertical length represents the temporal uncertainty. The lines represent the preferred interpretation of the slip offset history of the fault while respecting the constraints from the uncertainties.

Boxes 2a, 2b, t2, t3 - Offset of Oligocene conglomerates in Canton Canyon and Piru Creek

Crowell (2003) estimated that the “Sespe conglomerates” in Canton Canyon were offset ~75 km from their interpreted source area in the western SGM. Crowell (2003) interprets that the Sespe conglomerates were deposited before 28 Ma along the scarp of a normal fault before the basin was translated (Fig. 4B, box 2a). In contrast, Powell (1993) interpreted that the Sespe conglomerates in Canton Canyon are Oligocene in age and deposited prior to strike-slip movement on the SGCF and subsequently offset 42–46 km (Fig. 4B, box 2b).

This study also uses the offset the Sespe conglomerates, here interpreted as the Vasquez Formation and represented by samples t2 and t3, and their source areas (Fig. 4B, box t2) to restore the Ventura Basin. The Vasquez Formation was deposited between 25–21 Ma in its type section in the Soledad Basin based on biostratigraphy and K-Ar dates on plagioclase (Hendrix and Ingersoll, 1987), and we assume the same age range for t2 and t3. However, we recognize the uncertainty in correlating between basins, so the outline of box t2 is dashed due to poor age constraints. Detailed information about the interpreted age of the Vasquez Formation is provided (Supplemental Material). We interpret the change from SGA-only sediment in t2 to the addition of a significant contribution of LG in t3 as evidence that the basin had moved along the SGCF between t2 and t3 deposition. The blue solid line (Fig. 4B) shows our preferred

interpretation that the basin was moving prior to deposition of t3, and box t3 (Fig. 4B) displays the uncertainty in both the depositional age of sample t3 and the location of the basin during deposition. Also, box t3 is dashed due to the possibility that the contribution of LG to sample t3 is caused by changes in sediment routing rather than fault movement.

Box t4 – Offset of Vaqueros Formation (t4) and crystalline sources surrounding the Soledad Basin

We interpret the change from the SGA-only sourced Vasquez Formation (t2) to contributions from multiple crystalline sources in the Vaqueros Formation (t4) to signal that the Ventura Basin had been translated to the north and was receiving sediment from sources surrounding the Soledad Basin. Although the exact location of the Ventura Basin at the time is uncertain, this change suggests that the basin was north of the SGA during deposition of t4. The diminishing contribution of SGA from t4–t6 suggests that the Ventura Basin was likely proximal to the SGA during deposition of t4 and moving farther away from the SGA during deposition of t5 and t6. This is intuitive but speculative, and thus the spatial uncertainty brackets the basin location between where the SGA is closest to the SGCF and a location parallel to the Soledad Basin but still proximal to the SGA (Fig. 4B, box t4).

The reported age range of the Vaqueros Formation (t4) is between 27.5 Ma (Prothero, 2001) and 17 Ma (Prothero and Donohoo, 2001); its base is interpreted as Oligocene based on biostratigraphy (Blake, 1983) at Big Mountain, California, 20 km south of the study area (Fig. 1). The age of the overlying Rincon Shale is interpreted as >20 Ma near Santa Barbara, California (Prothero, 2001). We assume that the Vaqueros Formation at Lake Piru is between 25–20 Ma based on regional correlations of the base of the Rincon Shale and the top of the underlying Vasquez Formation; the blue line represents our preferred slip-history model (Fig. 4B). However, we recognize the uncertainty in these correlations, and we place a conservative age range of 27.5–18 Ma (Fig. 4B, box t4), which honors the oldest reported age of the Vaqueros Formation at Big Mountain. The 18 Ma minimum age uncertainty bound assumes that the Vaqueros Formation is older than the 17.4 Ma base of the Modelo Formation and that the 600 m of Rincon Shale represents at least 0.6 Myr of deposition. Detailed information about the interpreted age of the Vaqueros Formation is provided (Supplemental Material).

Box t5 – Presence of Oligocene zircon within the Miocene lower Modelo Formation

Zircon analyzed from sample t5 from the lower Modelo Formation yielded two Oligocene dates of 23 ± 1 Ma and 22 ± 1 Ma. No known igneous intrusive or metamorphic units of that age exist near the SGCF, but late Oligocene volcanic units are within the Vasquez Formation in the Soledad Basin (Hendrix and Ingersoll, 1987; Frizzell Jr and Weigand, 1993). This suggests that during deposition of t5,

a fluvial system within the Soledad Basin was supplying sediment across the SGCF to the eastern Ventura Basin and this is supported by the occurrence of Oligocene zircon in Soledad Basin sediments (Hoyt et al., 2018). Therefore, the spatial uncertainty is conservatively placed as the current north and south boundaries of the Soledad Basin (Fig. 4B, box t5) which results in a slip estimate of 12–30 km. The age uncertainty is interpreted as 13.9–17.4 Ma, which is the depositional age of the lower Modelo Formation (Yeats et al., 1994).

Boxes 6a, 6b, 6c, t6 – Offset of Devil Canyon conglomerate of the Miocene upper Modelo Formation

Boulders of gabbro, anorthosite, gneiss, and the Triassic Mount Lowe Granodiorite in the Devil Canyon conglomerate of the Miocene Modelo Formation have been used by several studies to infer that the Ventura Basin was right laterally offset from interpreted source regions in the SGM (Powell, 1993; Yeats et al., 1994; Crowell, 2003). However, each model interprets a different total offset and age. Crowell (2003) estimates the age of the Devil Canyon conglomerate between ca. 9 and 6.5 Ma and estimates ~45 km of offset (Fig. 4B, box 6a). Powell (1993) interprets these conglomerates to be 13–10 Ma and suggests an offset of 13 km along the Canton fault (Fig. 4B, box 6b) and the spatial uncertainty is calculated simply by subtracting 13 km from the 42–46 km range of total offset given by Powell (1993). Yeats et al. (1994) interprets a 10–5 Ma age range for the Devil Canyon conglomerate and an offset of 35–56 km (Fig. 4B, box 6c).

The Devil Canyon conglomerate is not present at the location where sample t6 was collected, and correlation between the upper Miocene Modelo Formation in these two locations is difficult due to local structural complexities. At Lake Piru, the upper Modelo Formation is interpreted as 13.9–6.5 Ma in age (Blake, 1991; Yeats et al., 1994) (Fig. 4B, box t6). This conservative age uncertainty overlaps with the age interpretations of all three of the previously published models, because we do not have high resolution age control on sample t6. Similarly, while the modeled mixture of parent contributions to samples t4–t6 is variable (Fig. 3), all are interpreted to have been sourced from crystalline units surrounding the Soledad Basin. Although we interpret this variability is caused by right-lateral offset, changes in sediment routing cannot be ruled out as a cause for changes in source-terrane abundance. For this reason, we conservatively use the boundaries of the Soledad Basin as the spatial uncertainty (Fig. 4B, box t6), which results in an offset of 12–30 km.

Boxes 8a, 8b – Offset of Hasley conglomerate of the Towsley Formation in the Ventura Basin

Both Crowell (2003) and Yeats et al. (1994) used pebbles and boulders found in the Hasley conglomerate (part of the lower Towsley Formation) as evidence that sediment was sourced from the SGM. Crowell (2003) reported these clasts as similar to those from the underlying Devil Canyon

conglomerate and interpreted right-lateral offset of ~25 km for these ~6.4 Ma beds (Fig. 4B, box 8a). Yeats et al. (1994) estimated the age of the Hasley conglomerate to be 10–5 Ma but estimated ≥ 30 km of slip to restore the same unit to the interpreted source region at the northern edge of the SGM (Fig. 4B, box 8b).

Box 9 – No offset of Fernando Formation across San Gabriel Fault

Yeats et al. (1994) observed no offset in the upper Fernando Formation, which is considered equivalent to the Pico Formation (t7) in this study (*sensu* Dibblee, 2010). Yeats et al. (1994) interpreted the top of the Fernando Formation to be <2 Ma and this age is used as the last possible fault movement of the SGCF (Fig. 4B, box 9).

Explanation of piercing points from other basins

Boxes 10a, 10b – Offset of Frazier Mountain and western SGM

Two studies use Frazier Mountain and similar igneous and metamorphic rocks in the western SGM to estimate total offset on the SGCF, but faulting and multiple igneous intrusions within these basement blocks have created various interpretations of how to restore them. For example, Powell (1993) restored Frazier Mountain 42–46 km southward along the San Gabriel fault (Fig. 4B, box 10a). Yeats et al. (1994) estimated 60 km of offset between the Mendenhall Gneiss of Frazier Mountain and the SGM, but does not provide an uncertainty for this slip estimate, so it is kept consistent with the 4 km estimate of Powell (1993) (Fig. 4B, box 10b). The youngest rocks in these basement blocks are Cretaceous, and therefore do not provide helpful age control for fault movement but are included as brackets (Fig. 4B, box 10a, 10b) because of their use in these models.

Boxes 11a, 11b – Offset of the Caliente and Mint Canyon Formations and their textural similarities

Both Crowell (2003) and Hoyt et al. (2018) interpret the Caliente Formation in the Plush Ranch Basin and the Mint Canyon Formation in the Soledad Basin as correlative due to similarities in texture, mineralogy, and petrology (Ehlert, 2003). These units were interpreted to have been deposited prior to initiation of fault movement and used to estimate offset along the San Gabriel fault (Crowell, 2003; Hoyt et al., 2018). Crowell (2003) estimates the age of the Mint Canyon and Caliente Formations as 16–11 Ma and restores them ~75 km (Fig. 4B, Box 11a), adding ~15 km of offset from previous estimates of 60 km (Crowell, 1954, 2003).

Hoyt et al. (2018) suggested that the Caliente Formation was deposited between 18–8 Ma based on biostratigraphy and magnetic stratigraphy (Prothero et al., 2008) and that the Mint Canyon Formation was deposited between ca. 14–10 Ma citing biostratigraphy data (Stirton, 1933) and zircon fission track dates of 11.6 ± 1.2 Ma and 10.1 ± 0.8 Ma (Terres and Luyendyk, 1985). Hoyt et al. (2018) interpret the age uncertainty in the model as the range between oldest age of the Caliente Formation (18 Ma) and the youngest

age of the Mint Canyon Formation (10 Ma) and a preferred offset estimate of 60–70 km (Fig. 4B, box 11b). However, Hoyt et al. (2018) recognized that total slip estimates of ~42–60 km cannot be ruled out based on petrography and detrital zircon geochronology data.

Boxes 12a, 12b – Offset of the Miocene Violin Breccia in Ridge Basin

The Miocene Violin Breccia in Ridge Basin interfingers with the Castaic, Peace Valley, and Hungry Valley Formations and is interpreted to be sourced from the Frazier Mountain area (Powell, 1993; Crowell, 2003). Crowell (2003) interpreted the age of the Violin Breccia as 10–5 Ma and that the oldest beds are offset ~45 km from their source (Fig. 4B, box 12a).

Both Crowell (2003) and Powell (1993) interpreted the Violin Breccia to record the entire fault history. Powell (1993) interpreted the formations that interfinger with the Violin Breccia to be 10–6 Ma (Fig. 4B, box 12b) and that the oldest beds of the Violin Breccia are offset 42–45 km from their source area in the Frazier Mountain block, assigning 21–23 km of slip to the San Gabriel fault between 10–6 Ma, ~13 km to the Canton fault between 13–10 Ma (Fig. 4B, box 12b), and <13 km to offset occurring after 6 Ma.

Box 13 – No offset of the Hungry Valley Formation in Ridge Basin

Beds of the Hungry Valley Formation are not offset across the San Gabriel fault (Crowell, 2003). Deposition of these beds is assumed to postdate movement on the San Gabriel fault, but no age uncertainty is given (Fig. 4B, box 13).

Implications for southern California tectonic reconstructions

Our preferred model suggests that the progression from t2 to t3 represents the Ventura Basin moving northward along the SGCF (Fig. 4B). This preferred timing of fault initiation between 25 and 21 Ma would predate all previous estimates of initiation of the SGCF by at least 3 Ma (Supplemental Material, Table S5) and is dependent on the depositional ages of the Vasquez and Vaqueros Formations (t2–t4) at Lake Piru but is in agreement with previous models that suggest the San Andreas transform began after 28 Ma (Atwater, 1989; Gooley et al., 2020). Two previous models (Powell, 1993; Crowell, 2003) were used to interpret a later SGCF initiation, but use the mineralogical similarities between this unit and the SGM to interpret offset. Our total slip estimate of 35–60 km (Fig. 4B) is in agreement with the 42–46 km estimate of Powell (1993), but the >60 km of offset interpreted by Crowell (2003) is not required to source the t2 and t3 sediment mixtures. Similarly, our model only partially overlaps with the 60–70 km preferred estimate of Hoyt et al. (2018) using offset of the Mint Canyon and Caliente Formations. Even if the change in DZ dates from t2 to t3 is caused by changes in sediment routing prior to translation, the consistent contribution of MG within samples t4–t7 suggests that the Ventura Basin was receiving

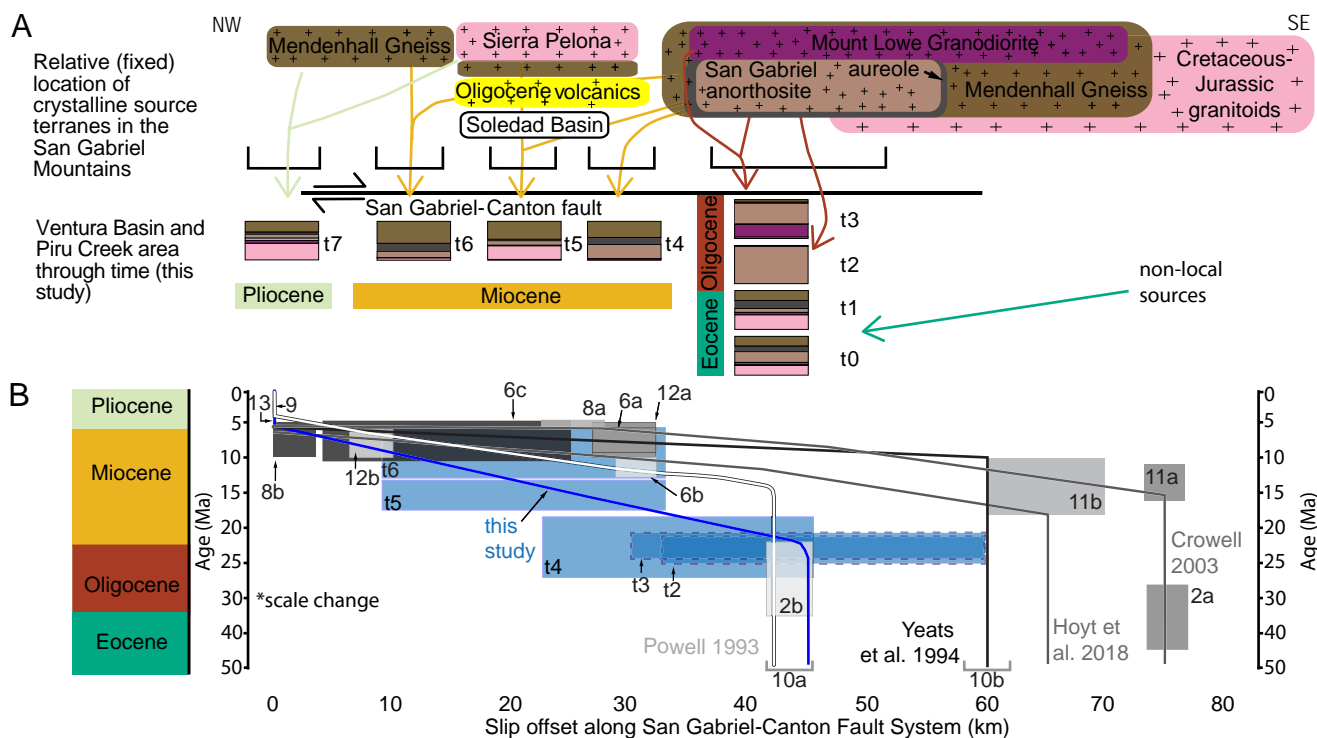


Figure 4: Compilation of the translational history of the Ventura Basin. A) Interpreted patterns of sediment routing and basin translation through time. Stacked bar charts show child sample DZ dates colored by parent age bins. B) Fault slip-offset diagram comparing our model that suggests 35–60 km of total slip to four published Ventura Basin reconstructions. Boxes represent fault slip uncertainty when reported and those with the same number in the label represent a different interpretation of the same piercing point (e.g. 2a, 2b, t2). Boxes constraining our model are colored blue and are labeled t2–t6 for consistency with the sample names. Boxes t2 and t3 are dashed because they represent interpretations with poor constraints.

sediment from the Soledad Basin rather than from MG-age rocks south of the SGA by time t4 (Fig. 4B). We conservatively interpret the range of uncertainty of fault timing as 27.5–18 Ma (Fig. 4B, box t4). Therefore, our latest SGCF initiation estimate of 18 Ma is equal to the earliest published estimate (Hoyt et al., 2018). The discrepancy between our model using the Ventura Basin and estimates using the Plush Ranch and Soledad basins (Hoyt et al., 2018) is currently unresolved. However, Hoyt et al. (2018) recognized that slip estimates between 42–60 km cannot be ruled out due to ambiguity in the sediment provenance data. This discrepancy could exist if each basin underwent different amounts of off-fault deformation during Pliocene transpression (Powell, 1993; Yeats et al., 1994) or because sediments with multiple parent components likely have higher spatial uncertainty compared to those with only one component. However, a more comprehensive regional study is required to resolve this issue.

Offset of the Devil Canyon conglomerate of the upper Miocene upper Modelo Formation (Fig. 1B) is used by three previous models to infer that the Ventura Basin was adjacent to its interpreted source area in the SGM by the time of deposition. However, we interpret the occurrence of Oligocene zircon in sample t5 to suggest that by the time of deposition of the middle Miocene lower Modelo Formation between 17.4–13.9 Ma (Yeats et al., 1994), the Ventura

Basin had already translated 12–30 km along the SGCF and was receiving sediments from Oligocene volcanic sources in the Soledad Basin (Fig. 4B, box t5). Although our interpretation of the model results indicates that the fault initiated before 18 Ma, our slip estimate using the offset of the lower Modelo Formation is in agreement with the 13 km estimate of (Powell, 1993) but is not in agreement with the 35–56 km estimate of Yeats et al. (1994) or the ≥ 45 km estimate of Crowell (2003). The wide range of interpretations in previous models suggest that the location of the Ventura Basin during the middle–late Miocene cannot be determined with high confidence, and our conservative approach better honors these uncertainties. Dense spatial and temporal sampling of the Oligocene and Miocene units in the Ventura Basin paired with studies investigating fault kinematics and off-fault deformation may provide higher resolution fault slip estimates.

CONCLUSIONS

Automated mineralogy data and mixture modeling of DZ age distributions reveal a previously unrecognized, singular sediment source of an Oligocene unit in the Ventura Basin, southern California. Drastic differences in sedimentology, sandstone mineral abundance, and zircon age spectra between the Oligocene sediments at Lake Piru and the

Sespe Formation in its type section nearby suggest that this unit was not part of the Sespe fluvial system but more similar to the alluvial Vasquez Formation of the Soledad Basin. Most significantly, two samples from this unit have distributions of DZ dates and abundant plagioclase that strongly suggest local sourcing primarily from the SGA. Our reassessment of these sedimentary deposits and their sources redefines the placement of a more appropriate piercing point prior to initiation of the SGCF. The reemergence of multiple DZ components following deposition of the Vasquez Formation is consistent with continued northward translation of the Ventura Basin and the sourcing of sediments from crystalline units exposed north of the SGA. These results support a reconstruction with 35–60 km of slip along the San Gabriel-Canton fault with fault slip occurring as early as Oligocene time, which is earlier than previous estimates.

ACKNOWLEDGMENTS

We thank the Chevron Center of Research Excellence at Colorado School of Mines (core.mines.edu) for funding support, Jacob Covault and Elisa Medri for field assistance, and Katharina Pfaff, Greg Gordon, Barry Shaulis, Ray Ingersoll, and Carl Jacobson for insightful discussions. Any use of trade, firm, or product names is for descriptive purposes only and does not imply endorsement by the U.S. Government.

Copyright notice

©The Author(s) 2021. This article is distributed under the terms of the [Creative Commons Attribution 4.0 International License](https://creativecommons.org/licenses/by/4.0/).

Literature Cited

- Atwater, T. (1989). Plate tectonic history of the northeast Pacific and western North America. In Winterer, E. L., Hussong, D. M., and Decker, R. W., editors, *The Eastern Pacific Ocean and Hawaii*, pages 21–72. The Geology of North America Volume N.
- Barth, A. P., Tosdal, R. M., Wooden, J. L., and Howard, K. A. (1997). Triassic plutonism in southern California: Southward younging of arc initiation along a truncated continental margin. *Tectonics*, 16(2):290–304.
- Barth, A. P., Wooden, J. L., and Coleman, D. S. (2001). SHRIMP-RG U-Pb zircon geochronology of Mesoproterozoic metamorphism and plutonism in the southwesternmost United States. *The Journal of Geology*, 109(3):319–327.
- Barth, A. P., Wooden, J. L., Howard, K. A., Richards, J. L., Wright, J., and Shervais, J. (2008). Late Jurassic plutonism in the southwest US Cordillera. In Wright, J. E. and Shervais, J. W., editors, *Ophiolites, Arcs, and Batholiths: A Tribute to Cliff Hopson*, volume 438, pages 379–396. Geological Society of America Special Papers 438.
- Blake, G. H. (1983). Benthic foraminiferal paleoecology and biostratigraphy of the Vaqueros Formation, Big Mountain area, Ventura County, California. In Squires, R. R. and Filewicz, M. V., editors, *Cenozoic Geology of the Simi Valley Area, Southern California*. Pacific Section, SEPM Society for Sedimentary Geology.
- Blake, G. H. (1991). Review of the Neogene biostratigraphy and stratigraphy of the Los Angeles Basin and implications for basin evolution. In Biddle, K. T., editor, *Active Margin Basins*, pages 135–184. American Association of Petroleum Geologists Memoir 52.
- Bohannon, R. G. (1975). Mid-Tertiary conglomerates and their bearing on transverse range tectonics, Southern California. *California Division of Mines and Geology Special Report Number 118*, pages 75–82.
- Crowell, J. C. (1954). Strike-slip displacement of the San Gabriel fault, southern California. *Geology of Southern California*, 170:49–52.
- Crowell, J. C. (1962). *Displacement along the San Andreas fault, California*, volume 71. Geological Society of America.
- Crowell, J. C. (1982). The Tectonics of Ridge Basin, Southern California. In Crowell, J. C. and Link, M. H., editors, *The Tectonics of Ridge Basin, Southern California*, pages 25–42. Pacific Section, SEPM Society for Sedimentary Geology.
- Crowell, J. C. (2003). Tectonics of Ridge Basin region, southern California. In Crowell, J. C., editor, *Evolution of Ridge Basin, Southern California: An Interplay Of Sedimentation And Tectonics*, pages 157–204. Geological Society of America Special Papers 367.
- Dibblee, T. W. (2010). *Geologic map of the Cobblestone Mountain Quadrangle, Ventura and Los Angeles counties, California: Dibblee Geology Center Map #DF-62: First Printing, 1996: Second Printing, 2010*. Santa Barbara Museum of Natural History, <http://www.sbnature.org/>.
- Ehlert, K. W. (2003). Tectonic significance of the middle Miocene Mint Canyon and Caliente formations, southern California. pages 113–130.
- Frizzell Jr, V. A. and Weigand, P. W. (1993). Whole-rock K-Ar ages and geochemical data from middle Cenozoic rocks, southern California: A test of correlations across the San Andreas fault. In Powell, R. D., Weldon II, R. J., and Matti, J. C., editors, *The San Andreas Fault System: Displacement, Palinspastic Reconstruction, And Geologic Evolution*, pages 273–288. Geological Society of America Memoir 178.
- Gooley, J. T., Sharman, G. R., and Graham, S. A. (2020). Reconciling along-strike disparity in slip displacement of the San Andreas fault, central California, USA. *GSA Bulletin*.
- Hart, N. R., Stockli, D. F., and Hayman, N. W. (2016). Provenance evolution during progressive rifting and hyperextension using bedrock and detrital zircon U-Pb geochronology, Mauléon Basin, western Pyrenees. *Geosphere*, 12(4):1166–1186.
- Hartley, A. J., Weissmann, G. S., Nichols, G. J., and Warwick, G. L. (2010). Large distributive fluvial systems: characteristics, distribution, and controls on development. *Journal of Sedimentary Research*, 80(2):167–183.
- Hendrix, E. D. and Ingersoll, R. V. (1987). Tectonics and alluvial sedimentation of the upper Oligocene/lower Miocene Vasquez Formation, Soledad basin, southern California. *GSA Bulletin*, 98(6):647–663.
- Hoyt, J. F., Coffey, K. T., Ingersoll, R. V., and Jacobson, C. E. (2018). Paleogeographic and paleotectonic setting of the middle Miocene Mint Canyon and Caliente formations, southern California: An integrated provenance study. In Ingersoll, R. V., Lawton, T. F., and Graham, S. A., editors, *Tectonics, Sedimentary Basins, and Provenance: A Celebration of the Career of William R. Dickinson*, pages 463–480. Geological Society of America Special Paper 540.
- Ingersoll, R. V. and Rumelhart, P. E. (1999). Three-stage evolution of the Los Angeles basin, southern California. *Geology*, 27(7):593–596.
- Ingersoll, R. V., Spafford, C. D., Jacobson, C. E., Grove, M., Howard, J. L., Hourigan, J., and Pedrick, J. (2018). Provenance, paleogeography and paleotectonic implications of the mid-Cenozoic Sespe Formation, coastal southern California, USA. In Ingersoll, R. V., Lawton, T. F., and Graham, S. A., editors, *Tectonics, Sedimentary Basins, and Provenance: A Celebration of the Career of William R. Dickinson*, pages 441–462. Geological Society of America Special Paper 540.
- Jacobson, C. E., Grove, M., Pedrick, J. N., Barth, A. P., Marsaglia, K. M., Gehrels, G. E., and Nourse, J. A. (2011). Late Cretaceous–early Cenozoic tectonic evolution of the southern California margin inferred from provenance of trench and forearc sediments. *GSA Bulletin*, 123(3–4):485–506.
- Jennings, C. W. (2010). *Geologic map of California, with modifications by Carlos Gutierrez, William Bryant, George Saucedo and Chris Wills*. Department of Conservation, California Geological Survey.
- Malkowski, M. A., Sharman, G. R., Johnstone, S. A., Grove, M. J., Kimbrough, D. L., and Graham, S. A. (2019). Dilution and propagation of provenance trends in sand and mud: Geochemistry and detrital zircon geochronology of modern sediment from central California (USA). *American Journal of Science*, 319(10):846–902.
- Powell, R. E. (1993). Balanced palinspastic reconstruction of pre-late Cenozoic paleogeology, southern California: Geologic and kinematic constraints on evolution of the San Andreas fault system. In Powell, R. D., Weldon II, R. J., and Matti, J. C., editors, *The San Andreas Fault System: Displacement, Palinspastic Reconstruction, and Geologic Evolution*, pages 1–106. Geological Society of America Memoir 178.

- Prothero, D. R. (2001). Chronostratigraphic calibration of the Pacific Coast Cenozoic: A summary. In Prothero, D. R., editor, *Magnetic Stratigraphy of the Pacific Coast Cenozoic*, pages 377–394. Pacific Section, SEPM Society for Sedimentary Geology, Book 91.
- Prothero, D. R. and Donohoo, L. L. (2001). Magnetic stratigraphy of the lower Miocene (early Hemingfordian) Sespe-Vaqueros Formations, Orange County, California. In Prothero, D. R., editor, *Magnetic Stratigraphy of the Pacific Coast Cenozoic*, pages 242–253. Pacific Section, SEPM Society for Sedimentary Geology, Book 91.
- Prothero, D. R., Kelly, T. S., McCardel, K. J., and Wilson, E. L. (2008). Magnetostratigraphy, biostratigraphy, and tectonic rotation of the Miocene Caliente Formation, Ventura County, California. *New Mexico Museum of Natural History and Science Bulletin*, 44:255–272.
- Rumelhart, P. E. and Ingersoll, R. V. (1997). Provenance of the upper Miocene Modelo Formation and subsidence analysis of the Los Angeles basin, southern California: Implications for paleotectonic and paleogeographic reconstructions. *GSA Bulletin*, 109(7):885–899.
- Saylor, J. E. and Sundell, K. E. (2016). Quantifying comparison of large detrital geochronology data sets. *Geosphere*, 12(1):203–220.
- Sharman, G. R., Graham, S. A., Grove, M., and Hourigan, J. K. (2013). A reappraisal of the early slip history of the San Andreas fault, central California, USA. *Geology*, 41(7):727–730.
- Sharman, G. R., Graham, S. A., Grove, M., Kimbrough, D. L., and Wright, J. E. (2015). Detrital zircon provenance of the Late Cretaceous–Eocene California forearc: Influence of Laramide low-angle subduction on sediment dispersal and paleogeography. *GSA Bulletin*, 127(1–2):38–60.
- Sharman, G. R. and Johnstone, S. A. (2017). Sediment unmixing using detrital geochronology. *Earth and Planetary Science Letters*, 477:183–194.
- Stirton, R. A. (1933). Critical review of the Mint Canyon mammalian fauna and its correlative significance. *American Journal of Science*, 5(156):569–576.
- Sylvester, P. J. (2012). Use of the mineral liberation analyzer (MLA) for mineralogical studies of sediments and sedimentary rocks. *Mineralogical Association of Canada*, 1:1–16.
- Terres, R. R. and Luyendyk, B. P. (1985). Neogene tectonic rotation of the San Gabriel region, California, suggested by paleomagnetic vectors. *Journal of Geophysical Research: Solid Earth*, 90(B14):12467–12484.
- Yeats, R. S., Huftile, G. J., and Stitt, L. T. (1994). Late Cenozoic tectonics of the east Ventura basin, Transverse Ranges, California. *AAPG Bulletin*, 78(7):1040–1074.

Identifying elusive piercing points along the North American transform margin using mixture modeling of detrital zircon data from sedimentary units and their crystalline sources

J. Clark Gilbert^{1,*}, Zane R. Jobe¹, Samuel A. Johnstone² and Glenn R. Sharman³

¹Department of Geology and Geological Engineering, Colorado School of Mines, Golden, CO 80401 USA

²U.S. Geological Survey, Geosciences and Environmental Change Science Center, Denver, CO 80225 USA

³Department of Geosciences, University of Arkansas, Fayetteville, AR 72701 USA

SUPPLEMENTAL DOCUMENTATION

Disclaimer: Any use of trade, firm, or product names is for descriptive purposes only and does not imply endorsement by the U.S. Government.

External contents:

[Gilbert-et-al-supplementary-data.zip](#), which contains the following datasets:

1. Table S1 is an Excel Workbook entitled "TableS1_Gilbert-et-al-supplementary-materials_zircon_u-pb_data_reduction.xlsx"
2. Table S2 is an Excel Workbook entitled "TableS2_Gilbert-et-al-supplementary_material_Zircongeochemistrydata.xlsx"

Internal contents:

1. Data and Methods
2. Table S3: Mixture Model Results
3. Table S4: Automated Mineralogy Modal Abundances
4. Table S5: Published Reconstructions

DATA AND METHODS

Detrital Zircon Geochronology

Mineral separation

Sample preparation at Colorado School of Mines included a jaw crusher and disc mill for grain disaggregation and density separation on a Wilfley Table. The heaviest fraction was run over a slope Frantz magnetic separator set to 0.2–1.6 Amps in 0.2 Amp increments to remove any ferromagnetic minerals. The zircon grains were then separated using heavy (> 2.85 g/cc) liquid methods (Methylene Iodide).

U-Pb LA-ICP-MS Analysis

The geochronology data for samples analyzed for this study were collected at the University of Arkansas TRAIL Lab (<https://icp.uark.edu/the-ub-geochronology/>) using their ESI NWR 193nm Excimer Laser Ablation System and Thermo Scientific iCapQ Quadrupole Mass Spectrometer. Zircon grains were mounted on double-sided tape and chosen at random for analysis. The data were collected using the following laser and mass spectrometer settings: 25 micron spot size, 200 shot bursts (10Hz rep rate for 20 seconds), ~15 second gas blank, and then washout (total analysis length is about 50 seconds), 800 mL/min He flow, and a power setting of 40% and a fluence (energy of laser divided by area of illumination) of ~3.5 J/cm². The following samples were run with n=120 grains in November of 2018: upper Modelo (t6), lower Modelo (t5), Vaqueros (t4), basal Vasquez (t2), Matilija (t1) and Juncal (t0) Formations. Samples from the

*Corresponding author: jclarkgilbert@gmail.com

Vasquez (t3) and Pico (t7) Formations were run in June 2019 and n=150 grains were selected. The analysis used Plešovice (Sláma et al., 2008) as primary standard, 91500 (Wiedenbeck et al., 1995) as secondary standard and R33 (Black et al., 2004) as tertiary (backup) standard. Five analyses of the primary standard, then five secondary standards were repeated three times for calibration. Throughout the rest of the analyses, 10 samples were shot, followed by 1 tertiary, secondary and primary standard, then 10 more samples followed by only the secondary and primary standards. This pattern was repeated for the all analyses.

Data were reduced using Iolite software and the excel template named “Zircon U-Pb Data Reduction Template.xls” originally created by Lisa Stockli, Owen Anfinson and modified by Kelly Thomson (Table S1). For zircon <1300 Ma, the $^{206}\text{Pb}/^{238}\text{U}$ ages were used and for zircon >1300 Ma, the $^{207}\text{Pb}/^{206}\text{Pb}$ ages were used. Several age cutoffs were tested, but the 1300 Ma cutoff best displayed the distinct geochronological signature of each parent source. The only apparent difference when using younger age cutoffs was that the approximately 1200 Ma zircon present in sample t2 had several small peaks between 1200–900 Ma with unusual isochron estimations that were attributed to Pb loss. Barth et al. (1995) also reported these finding in the San Gabriel anorthosite from SHRIMP microprobe ages. Discordant grains were discarded using the following cutoff parameters: 30% $^{206}\text{Pb}/^{238}\text{U}$ – $^{207}\text{Pb}/^{206}\text{Pb}$ discordance filter for $^{207}\text{Pb}/^{206}\text{Pb}$ ages, -15% $^{206}\text{Pb}/^{238}\text{U}$ – $^{207}\text{Pb}/^{206}\text{Pb}$ reverse discordance filter for $^{207}\text{Pb}/^{206}\text{Pb}$ ages, 10% error cutoff for $^{206}\text{Pb}/^{238}\text{U}$ ages, and 15% $^{206}\text{Pb}/^{238}\text{U}$ – $^{207}\text{Pb}/^{235}\text{U}$ discordance filter for $^{206}\text{Pb}/^{238}\text{U}$ ages. After data reduction, we found that using 91500 as the primary standard resulted in ages much closer to those of our parent source ages from the literature. Both the $^{206}\text{Pb}/^{238}\text{U}$ age (1062.4 ± 0.8 Ma) and $^{207}\text{Pb}/^{206}\text{Pb}$ age (1065.4 ± 0.6 Ma) of the 91500 standard reported through CA-TIMS dating (Wiedenbeck et al., 1995) are much closer to the ~1200 Ma zircon in sample MN-16-08 than the Plešovice standard ($^{206}\text{Pb}/^{238}\text{U}$ age = 337.16 ± 0.6 Ma, $^{207}\text{Pb}/^{206}\text{Pb}$ age = 337.96 ± 0.61 Ma, CA-TIMS) (Sláma et al., 2008). An equal number of 91500 and Plešovice analyses were collected, so the reduction only involved switching the primary and secondary standards and repeating the data reduction with the same parameters.

Sediment Mixture-Modeling

Selecting Parent Populations

All published zircon geochronology ages found in the region were originally included as parents in the mixture modeling. However, there were several instances where we decided to remove or combine published zircon populations as potential parent sources. As a sensitivity analysis, the parents were tried in many different combinations and those parents that never contributed to the children were disregarded as a potential source. The list of detrital zircon data sources used in the mixture modeling is included in Table S2.

Jurassic zircon ages are sparse in the area and Cretaceous zircon ages are found in many of the same areas due to the long history of the Farallon subduction zone. For this reason, we combined the Jurassic and Cretaceous ages together as one parent population, preferring higher numbers over spatial uniqueness.

Zircon from the Pelona Schist (exposed in the Sierra Pelona) have both Mesozoic and Paleoproterozoic age peaks (Jacobson et al., 2000), but only a small peak at ~1200 Ma, and no peaks between 1500–1300 Ma. The Sierra Pelona could be a sediment source for both Miocene and Pliocene samples (t4–t7). However, when included in the mixture models, it overfit the data and was therefore removed. For example, the mixture model for the Juncal (t0) and Matilija (t1) Formations included a significant percentage of Pelona Schist. This was interpreted as the model preferring one parent with two age populations that are very similar to two other parents (Cretaceous–Jurassic and the Mendenhall Gneiss). It is unlikely that the Sierra Pelona contributed to t0 or t1 because both detrital samples have zircon in the 1500–1300 Ma range and a several ~1200 Ma grains. Therefore, it is more likely that the Precambrian zircon in the detrital samples were sourced from the southern edge of the San Gabriel anorthosite and the aureole in the Mendenhall Gneiss and not from the distal Sierra Pelona.

Sediment Unmixing Modeling Program

A python script (i.e. Jupyter notebook) named VenturaBasinMixing.ipynb (<https://github.com/clarkgilbert/VenturaBasin-sediment-mixing>) was heavily modified from the Sediment Unmixing Modeling python package available at (Sharman and Johnstone, 2017). The program accepts detrital zircon data in the template of Table S2. The program uses a forward-modeling approach at estimating what mixture of a fixed number of parents likely contributed to a child population based on a predefined comparison metric. Here we use a forward model in an inverse approach by examining a large number of models with different parameters to find the best fitting parameters (mixing coefficients). Each parent is specific and predefined by looking at the available detrital zircon data in the region. The mixture models use the following equation

$$KDE_{Mix} = MixCoeff_1 * KDE_{P1} + MixCoeff_2 * KDE_{P2} + MixCoeff_n * KDE_{Pn} \quad (1)$$

where the output is a kernel density estimate (KDE_{Mix}). This best-fit mixture is the sum of each potential parent’s

kernel density estimate (KDE) multiplied by its mixture coefficient. The equation for the kernel density estimator can be expressed as (Silverman, 2018; Vermeesch, 2013):

$$KDE(x) = \frac{1}{nh} \sum_{i=1}^n K\left(\frac{x - x_i}{h}\right) \quad (2)$$

where in this case K is a Gaussian kernel and h is the bandwidth of 1.5 Ma. In this study, the Vmax value of the Kuiper statistic (Saylor and Sundell, 2016) is calculated for an entire distribution, and used to evaluate the goodness of fit for each. All of our forward mixture models would have a set of mixing coefficients, which are used to create the mixed PDP via Equation 1, and the single Vmax value is calculated between the entire observed PDP and the mixed PDP. We then try many combinations of mixture coefficients and find the mixture coefficient combination that produces the smallest Vmax. Every parent distribution is therefore present in every part of the mixed Vmax. However, some parent distributions might not have any grains at certain ages and are therefore zero. The mixture of each parent that contributed to a given child is reported in percent (Fig. 3) with a resolution of 0.01 (1%). The vertical separation between the child kernel density estimate (black line) and the best-fit mixture model (red dashed line) shows how closely the model fits the data. We used a method of resampling with replacement bootstrap method reported in Malkowski et al. (2019) as a sensitivity analysis and to report uncertainties within the best-fit mixtures. This permutation method randomly removes a zircon date from the given parent and child distributions and randomly substitutes another date in the distribution. This sensitivity analysis hints at how much changing the ages in our predefined parents affects our models. Peaks in the kernel density estimates defined by fewer zircon dates are typically more sensitive to the bootstrapping. Our study reports the permutation results for 10,000 iterations with an optimized search. However, a brute force search was conducted on 1,000 iterations as another test and the results did not change from those of the optimized search. Therefore, we assume that the optimized search is not arbitrarily ignoring portions of the distributions.

Reconciling ID-TIMS and LA-ICP-MS dates

Models that used parent distributions composed of zircon dates collected using high precision isotope dilution-thermal ionization mass spectrometry (ID-TIMS zircon) posed problems with mixture model results. When ID-TIMS dates reported by Barth et al. (1995) were used to create a parent distribution for the San Gabriel anorthosite (Fig. 2), the mean varied by up to 20 Ma from any calculated means of the age peaks from the child distributions of zircon dates collected from the LA-ICP-MS method. In effect the best-fit mixture model would include a contribution of the Triassic Mount Lowe Granodiorite even though no zircon dates of that age existed in the unimodal child population. We hypothesize that because the LA-ICP-MS dates are not within uncertainty of the high precision ID-TIMS dates, and they are comprised of younger dates, the model includes younger dates to skew the mean down. Luckily, Barth et al. (2001) also used sensitive high-resolution ion microprobe (SHRIMP) methods to reanalyze the same zircon previously analyzed by ID-TIMS methods. Calculated errors in SHRIMP dates used for the parent distribution for the San Gabriel anorthosite were similar to those in the child distribution of LA-ICP-MS zircon dates and were used to create the parent age distribution.

Sandstone Automated Mineralogy (SAM)

Standard thin sections (27 x 46 mm) were made from the same samples used for both detrital zircon geochronology and sandstone automated mineralogy (SAM) analysis with the exception of sample t7. No thin section was made for t7 because the sandstone was so disaggregated that it would need epoxy impregnation, which could introduce selection bias. Automated mineralogy analyses were conducted at the Automated Mineralogy Lab at Colorado School of Mines, using their TESCAN Integrated Mineral Analyzer (TIMA) system (<https://geology.mines.edu/laboratories/automated-mineralogy-laboratory/>). The model number for this system is Tescan-Vega-3 Model LMU VP-SEM. A 7 µm increment was chosen for the energy dispersive X-ray spectrometer (EDS) with a light cutoff of >35% to focus only on the heavy (brightest) minerals with a higher resolution. Acceleration voltage=24 keV and beam intensity=14 for all analyses.

Data reduction involved identifying minerals within the samples based on their chemical makeup (EDS response), and a proprietary mineral-model database at the Automated Mineralogy Lab was utilized. Samples from the following formations had ≥1% of unidentified minerals: Juncal (t0=4.6%), Vasquez (t3=1.0%), Vaqueros (t4=1.3%) and lower Modelo (t5=1.0%), while the other 4 had only trace (≤1%) amounts. Non-unique minerals or minerals with low concentrations were grouped by mineralogy (Table S4).

UNCERTAINTY IN THE DEPOSITIONAL AGES OF THE VASQUEZ AND VAQUEROS FORMATIONS

Vasquez Formation

The Oligocene coarse-grained red beds found north of Lake Piru and in Canton Canyon have historically been assigned to the Sespe Formation due to their stratigraphic position (Bohannon, 1975; Dibblee, 2010, 1989; Crowell, 2003). However,

Results of Mixture Modeling of Detrital Zircon Data

Function	Vmax	1000 iterations per model				
Parent name	N analyses	Vmax values		Modeled parent contributions (percent p50 (p2.5 - p97.5))		
Child name	N analyses	[p50 (p2.5 - p97.5)]	CJ	LG	SGA	MG
CJ	246					
LG	33					
SGA	35					
MG	39					
t7	131	0.35 (0.28 - 0.44)	0.44 (0.22 - 0.58)	5.13e-17 (0.0 - 0.06)	3.32e-17 (0.0 - 0.02)	0.55 (0.41 - 0.77)
t6	115	0.31 (0.19 - 0.46)	2.22e-16 (0.0 - 0.10)	1.73e-17 (0.0 - 0.01)	3.02e-17 (0.0 - 0.07)	1.0 (0.89 - 1.0)
t5	102	0.38 (0.26 - 0.51)	0.23 (0.13 - 0.44)	4.72e-17 (0.0 - 1.85e-13)	6.05e-17 (0.0 - 1.08e-13)	0.77 (0.56 - 0.87)
t4	118	0.29 (0.18 - 0.43)	7.07e-17 (0.0 - 0.1)	3.58e-17 (0.0 - 0.02)	0.06 (0.0 - 0.32)	0.92 (0.68 - 1.0)
t3	144	0.22 (0.16 - 0.30)	0.06 (7.64e-20 - 0.22)	0.367 (0.275 - 0.47)	0.49 (0.29 - 0.58)	0.08 (9.4e-21 - 0.22)
t2	118	0.34 (0.20 - 0.50)	1.68e-17 (0.0 - 0.03)	2.18e-17 (0.0 - 0.047)	0.94 (0.80 - 1.0)	0.05 (0.0 - 0.20)
t1	98	0.20 (0.14 - 0.28)	0.33 (0.16 - 0.47)	1.49e-06 (0.0 - 0.11)	4.47e-4 (0.0 - 0.15)	0.63 (0.46 - 0.79)
t0	112	0.19 (0.14 - 0.27)	0.23 (0.06 - 0.42)	0.09 (1.93e-18 - 0.21)	0.125 (1.13e-18 - 0.29)	0.56 (0.26 - 0.77)

Table S3: Results of the mixture modeling used in this study. The median (p50), and bounds on the 95% confidence interval (p2.5 and p97.5) are reported for both the Vmax values and modeled parent contributions for each bootstrapped model.

the finer-grained fluvial-deltaic deposits of the Sespe Formation were deposited further south from an extra-regional source in the Basin and Range province (Ingersoll et al., 2018). In contrast, the alluvial deposits near Lake Piru have clast sizes up to 7 m (Bohannon, 1975) and are similar to the Vasquez Formation at its type section in the Soledad Basin (Hendrix and Ingersoll, 1987). We interpret that the Oligocene deposits at Lake Piru are part of the Vasquez Formation, not the Sespe Formation.

The depositional age of the Vasquez Formation in the Soledad Basin is unknown because no diagnostic fossils have been reported. However, plagioclase within volcanic units near the base of the Vasquez Formation yielded potassium-argon (K-Ar) dates of 20.7 ± 0.8 (Woodburne, 1975), 24.5 ± 0.8 and 25.6 ± 2.1 Ma (Crowell, 1973). Hendrix and Ingersoll (1987) used these K-Ar dates and the recognition of early Miocene vertebrate fossils in the overlying Tick Canyon Formation to interpret that the Vasquez was deposited between 21 and 25 Ma. Frizzell Jr and Weigand (1993) reported a whole-rock K-Ar date of 23.6 Ma, which corroborated the previous dates of Crowell (1973), and interpreted that volcanism in the Vasquez Formation happened between 25.6–23.6 Ma (Hoyt et al., 2018).

Correlation of the Vasquez Formation between the Soledad and Ventura basins is difficult and we recognize this uncertainty. The Vasquez Formation in the Soledad Basin is >5000 m thick with volcanic units near its base, while at Lake Piru in the eastern Ventura Basin, it is only 90 m thick and does not contain recognizable volcanics. Despite these differences, we interpret that they are at least partially correlative due the similarities in grain size, composition, texture, mineralogy, and sedimentological structures between them. No fossils have been reported from the Vasquez Formation at Lake Piru, but we assume that it is older than 21 Ma, especially because the base of the overlying Vaqueros Formation is also interpreted to be Oligocene in the region.

Vaqueros Formation

The exact age of the Vaqueros Formation at Lake Piru is unknown and was interpreted from nearby studies. The age of the Vaqueros Formation has been debated since it was first described by Hamlin (1904) in Vaqueros Creek near Monterey, California. Unfortunately this nomenclature was used throughout California based on outdated biostratigraphic correlations until Thorup (1943) formalized the type section to include 600 m of marine sandstone and siltstone. Loel and Corey (1932) designated a “Vaqueros Formation” for the unit based on the presence of the gastropod species *Turritella inezana*, but did not honor strict stratigraphical constraints (Edwards, 1971). Addicott (1972) defined the “Vaqueros Stage” by adding other molluscs and designating it as late Oligocene to early Miocene (Blake, 1983). Two studies used magnetic stratigraphy to demonstrate that molluscs of the “Vaqueros Stage” are found in rocks as old as 27.5 Ma at Big Mountain

Mineral Name	Juncal	Matilija	basal_Vasquez	Vasquez	Vaqueros	lower_Modelo	upper_Modelo	Granite
	t0	t1	t2	t3	t4	t5	t6	
	MN-16-06*	MN-16-07*	MN-16-08*	MN-16-05*	MN-17-11*	EDF-17-1*	MN16-04*	CC-17-GR*
Quartz	32.1	43.1	6	13.2	41	38.6	38.7	36.1
Orthoclase	17.3	21.5	7.7	10.6	20.7	25	21.2	25.3
Plagioclase	27.9	28.1	57.1	60.1	28.3	28.6	32.5	32.6
Muscovite	1.3	1.5	0.8	0.9	1.8	0.9	1.5	3
Biotite	2.5	1	7.6	2.6	2.3	2.1	2.6	2.6
Chlorite	0.8	0.2	2.9	0.4	0.1	0	0.1	0
Apatite	0.2	0.1	1.5	0.5	0	0.1	0.2	0
Pyroxene/ Amphibole	0.1	0.6	6.2	6.2	0.8	0.3	0.7	0
Garnet	0.9	0.1	0.6	0.1	0.2	0.1	0	0
Epidote	0.7	1.6	2.2	1.9	0	0	0	0
Tourmaline	0.5	0	0	0	0.1	0.1	0	0
Other Silicates	1	0	0	0	0.1	0.1	0	0
Zircon	0	0	0	0	0	0	0	0
Titanite	0.1	0.1	0.4	0.2	0	0	0	0
Rutile	0.3	0.1	0.2	0.1	0.1	0.2	0.1	0
Ilmenite	0	0.1	1.9	0.5	0.3	0	0.2	0
Chromite	0	0	0	0	0	0	0	0
Fe oxides	0.3	0	0.6	0.1	0.1	0	0	0
Other oxides	0	0	0	0	0	0	0	0
Sulfates	0	0	0	0	0.1	0	0	0
Olivene	0	0	0.1	0	0.2	0	0	0
Other REE	0	0	0	0	0	0	0	0
Carbonates	7	0	0	0	0	0	0	0
Clay Minerals	2	1.3	2.5	1.4	2.3	3	1.3	0.1
Clinochlore	0.1	0	0.2	0.2	0	0	0	0
Ankerite+clay	0.1	0	0.1	0	0	0	0	0
[Unclassified]	4.5	0.6	1.2	0.9	1.3	1	0.7	0.1
Total	100	100	100	100	100	100	100	100

Table S4: Automated mineralogy reported as modal abundance (area percent of each mineral phase) for Ventura Basin samples. All analyses were completed on the TIMA platform at Colorado School of Mines. Original sample names used in field are denoted by asterisk (*).

20 km south of Lake Piru (Prothero et al., 1996), but as young as ~17 Ma in the Santa Ana Mountains (Prothero and Donohoo, 2001) approximately 110 km to the southeast. These studies demonstrated that the fauna of the Vaqueros stage lived between 28–17 Ma (late Oligocene to late Miocene) and therefore are not particularly useful as index fossils.

The following criteria were used to predict the age of the Vaqueros Formation in Piru Creek, and the implications that alternative hypotheses could have on the interpretations in this study. A detailed biostratigraphy study at Big Mountain (22 km to the south of the outcrop in Piru Creek determined that the lowest part of the section was late Zemorrian (late Oligocene) in age (Blake, 1983). However, this interpretation is based on shallow water benthic foraminifera that are difficult to correlate to other California stages based on deep-water bathyal fossils (Edwards, 1971; Blake, 1983). The fauna in the upper two members of the Vaqueros Formation at Big Mountain are equivalent to the lower Rincon Shale at Los Sauces Creek ~60 km to the west near Carpinteria, California (Edwards, 1971; Blake, 1983). The base of the Rincon Shale is interpreted as early Miocene 80 km to the west at the Tajiguas Landfill near Santa Barbara, California (Stanley et al., 1994) and (Prothero and Donohoo, 2001) interpreted this entire section of Rincon Shale to be either 23.2–22.2 Ma or 21.5–20.0 Ma based on magnetostratigraphy.

It is unclear if the section through the Vaqueros at Piru Creek are age-equivalent to the section at Big Mountain because the Vaqueros Formation is overlain by the Conejo Volcanics (Blundell, 1983) and the Rincon Shale is not present. The Conejo Volcanics have been K-Ar dated at 15.9 ± 0.8 Ma (Turner and Campbell, 1979) and have an Ar-Ar date range of 17.1–16.3 Ma (Weigand et al., 2002), which suggests that there was significant period of nondeposition or erosion between the two units. However, studies based on biostratigraphy (Blake, 1983) and magnetic stratigraphy (Prothero et al., 1996) support the conclusion that the base of the Vaqueros Formation is Oligocene at Big Mountain.

How the section of the Vaqueros Formation and the overlying Rincon Shale at Lake Piru correlates in age to other basins is currently unknown. Although the youngest reported age of the Vaqueros Formation is ~17 Ma, its top must be older than 17.4 Ma, which is the reported age of the base of the Modelo Formation at Lake Piru (Yeats et al., 1994). More than 600 m of Rincon Shale lies between these two surfaces. If this section is correlative to the section at Tajiguas Landfill, then the base of the Rincon Shale is at least 20 Ma (Prothero and Donohoo, 2001) and the top of the Vaqueros Formation is older than 20 Ma. The overlying Vasquez Formation at Lake Piru is between 21 and 25 Ma if it is equivalent to its type section in the Soledad Basin. Therefore, we assume that the depositional age of sample t4 from the Vaqueros Formation is older, likely between 25–20 Ma. However, due to the uncertainty in correlating to nearby sections, we use a conservative age range of 27.5–18 Ma for the Vaqueros Formation piercing point (box t4) described below.

PUBLISHED RECONSTRUCTIONS

Reference	Fault Name	Right Slip	Timing	Notes
Crowell (1954)	San Gabriel	60 km total		Restoring Alamo-Frazier Mountain to similar basement rocks in San Gabriel Mountains
Crowell (1962)	San Gabriel	35 km	Oligocene–Middle Miocene	Offset of Eocene and Oligocene ‘megabreccias’ in the Soledad Basin
Bohannon (1975)	San Gabriel	60 km total		Required to juxtapose the Oligocene Sespe conglomerates in Canton Canyon to the anorthosite and Mount Lowe Granodiorite source in the San Gabriel Mountains. Cites (Crowell, 1954)
Ehlig (1982)	San Gabriel	60 km total		
Ehlert (1982)	San Gabriel	60 km total	Miocene	Correlates upper part of the Mint Canyon and Caliente Formations with Chocolate Mountains based on the presence of rapakivi-textured clasts
Crowell (1982)	San Gabriel-Canton	60 km total	12 to ~14 Ma, ended at ~5 Ma	Claims timing is only valid if earlier fault offset the Sespe Conglomerates
Crowell (1982)	San Gabriel	55 km		Restore 25–30 Ma Sespe Conglomerates to their source region near the Big Tujanga Wash in the western San Gabriel Mountains
Crowell (1982)	Canton		10.5–8.5 Ma	
Powell (1993)	San Gabriel-Canton-Vasquez Creek fault	42–46 km total	12–13 Ma to present	Restores Frazier Mountain block to Mount Pinos and the eastern Orocopia Mountains
Powell (1993)	Canton	13 km	13–10 Ma	Assumes that the anorthosite bearing Modelo Formation is fully offset. However, if it is not fully offset, movement could have begun at 16–14 Ma based on finding no evidence of faulting before the end of the Saucian

Table S5: Summary of published restorations showing the timing and magnitude of slip along the San Gabriel–Canton fault system.

Powell (1993)	San Gabriel	21–23 km	10–6 Ma	Timing is based on fossil evidence of the age of units interfingering with the Violin Breccia in Ridge Basin and the distance that it is offset from its source area in Frazier Mountain
Powell (1993)	San Gabriel	3–5 km	6–4 Ma	
Powell (1993)	Vasquez Creek Fault	≤~5 km	6 Ma to present	Offset of quartz diorite units used as piercing points. Any restoration 5 km causes the units to misalign. Also known as the south branch of the San Gabriel Fault. Timing is based on offset of Pa-coima and Big Tujunga Canyons
Matti and Morton (1993)	San Gabriel	≤~44 km total		22 km on north branch based on restoring Mount Lowe Granodiorite 'tail' with main body, 22 km on south branch based on their "proposal that the fault has displaced the left-lateral Malibu Coast-Santa Monica-Raymond fault from the Evey Canyon-Icehouse Canyon fault in the southeastern San Gabriel Mountains"
Yeats et al. (1994)	San Gabriel	60 km total	10–5 Ma	Offset of the Precambrian Mendenhall Gneiss and anorthositic rocks from near Frazier Mountain and the western San Gabriel Mountains (Crowell, 1962; Ehlig and Crowell, 1982)
Yeats et al. (1994)	Canton	≥23 km	10 Ma	Canton Fault dies out in the Miocene Devil Canyon Conglomerate, meaning at least 23 km of slip happened prior to deposition
Yeats et al. (1994)	San Gabriel		Miocene because Mint Canyon Formation is offset (Ehlig et al., 1975; and Ehler, 1982)	60 km Alamo-Frazier source for breccia in Mint Canyon Formation in Soledad Basin. Timing of Initiation: Clarendonian and Barstovian vertebrate stage fossils and Tuff beds in the Mint Canyon. Zircon fission-track ages of 10.1 ± 0.08 Ma and 11.6 ± 1.2 Ma (J. Obradovich and T.H McCulloh in Terres Luyendyk, 1985)
Yeats et al. (1994)	San Gabriel	35–56 km	10–5 Ma	Right slip of at least 35 km but possibly as much as 56 km is required to place the lower Mohnian Devil Canyon Conglomerate next to its probable source in the San Gabriel Mountains
Yeats et al. (1994)	San Gabriel	35–60 km	10–5 Ma	Offset of gneiss clasts Violin Breccia in Ridge Basin to appropriate source area
Yeats et al. (1994)	Devil Canyon		10-5 Ma	Interprets that the Canton Fault rejoins the SGF north of the Castaic Hills oil field and therefore it cannot continue into the San Fernando Valley. He thinks that the Devil Canyon Fault could have taken some of that slip
Yeats et al. (1994)	San Gabriel	≥30 km	10–5 Ma	The apex of the Hasley submarine fan is offset at least 30 km from its inferred source region in the San Gabriel Mountains
Yeats et al. (1994)	San Gabriel	0 km	Pliocene >2 Ma	The upper Fernando Formation is correlative across the San Gabriel Fault, suggesting most of the fault movement on the northern strand ceased before then. However, he places some caveats on biostrat correlation, etc.
Yeats et al. (1994)		~10 km shortening	Post SGF movement	
Rumelhart and Ingersol (1997)	San Gabriel	50–60 km total	12 Ma–5 Ma	Timing: rapid sedimentation rates in the adjacent Los Angeles basin; Total slip: The Modelo Formation in the Santa Monica Mountains contains almost no Ca-rich plagioclase, suggesting that the Los Angeles basin was 50 km to the south and sediments from the SGA were blocked by the Simi Uplift and directed into the eastern Ventura Basin
Ingersol and Rumelhart (1999)	San Gabriel	60 km total	10–5 Ma	This publication is focused more on the transrotation. They just put 60 km of SGF slip and cite Crowell (1982)
Yeats (2001)				Miocene Caliente Formation of Lockwood Valley (Ehlig et al., 1975; Ehler, 1982)
Yeats (2001)		≥35 km		lower Mohnian Devil Canyon Conglomerate of the upper Modelo (Crowell, 2003)
Yeats (2001)		≥30 km		Uppermost Mohnian-"Delmontian" Hasley Conglomerate at the base of the Towsley Formation and source in San Gabriel Mountains
Nourse et al. (2002)	North branch of San Gabriel	22 km	~9-5 Ma	Necessary to restore the main Mount Lowe Granodiorite complex to its 'tail' south of the San Gabriel Fault. The 15 km of slip on the Sawpit Canyon-Clamshell fault would add offset east of this tail.

Table S5 (cont.): Summary of published restorations showing the timing and magnitude of slip along the San Gabriel–Canton fault system.

Nourse et al. (2002)	Sawpit Canyon-Clamshell fault	15 km		
Nourse et al. (2002)	South branch of San Gabriel		ca. 12 Ma and likely before north branch movement	
Crowell (2003)	San Gabriel-Canton	~75 km total	16–5 Ma	Alignment of the Caliente and Mint Canyon Formations, which would add another 15 km from the original offset of Frazier Mountain to the western San Gabriels
Crowell (2003)	Canton	~35 km	16–11 Ma	Offset of the Mint Canyon (Soledad Basin) and Caliente Formations (Plush Ranch Basin); older normal fault (possibly the Canton Fault) with no strike-slip component active prior to ca. 18 Ma to deposit the Sespe Conglomerates in Canton Canyon.
Crowell (2003)	San Gabriel	≥45 km	between ~11 Ma and 5 Ma (Crowell, 1986)	Offset of 6.5–9 Ma Devil Canyon Conglomerate to source area in the San Gabriel Mountains
Crowell (2003)	San Gabriel	~25 km	10–5 Ma	Offset of ~6.5 Ma Hasley Conglomerate to source area in the San Gabriel Mountains
Crowell (2003)	San Gabriel	~45 km	10–5 Ma	Offset of Violin Breccia in Ridge Basin to appropriate source area
Crowell (2003)	San Gabriel	0 km	~5 Ma	Beds of the Hungry Valley Formation are not offset by the San Gabriel Fault, whose deposition is assumed to postdate movement on the San Gabriel Fault.
Crowell (2003)	Alamo-Frazier Mountain	5 km shortening	post 5 Ma	Repetition of the belt of the Violin Breccia in the Hardluck slice
Yeats and Stitt (2003)	Canton	30 km		Offset of Sespe? Fine grained deposits in subsurface Placerita Oilfield to conglomerates in Piru Creek and Canton Canyon
Yeats and Stitt (2003)	San Gabriel			
Ingersoll et al. (2014)	San Gabriel	~40 km	12–6 Ma	Claims 12–6 Ma in abstract, but 12–5 Ma in text, citing Crowell, Hendrix, etc. No explanation for the change
Ingersoll et al. (2014)	Canton	~30 km	18–12 Ma	Cites Crowell (2003b) but moves slip initiation to 18 Ma to align with start of transrotation
Coffey et al. (2019)	Canton		18 Ma to after ca. 13 Ma	60–70 km total on San Gabriel-Canton Fault system
Coffey et al. (2019)	San Gabriel		sometime between 13 and 9 Ma	
Hoyt et al. (2018)	San Gabriel-Canton	~42 to ~70 km	San Gabriel 10–5 Ma; 18 Ma Canton	Partial similarities in petrology between Mint Canyon and Caliente Formations
Nourse et al. (2020)	San Gabriel	40–60 km	12–5 Ma	Cites others' work

Table S5 (cont.): Summary of published restorations showing the timing and magnitude of slip along the San Gabriel–Canton fault system.

Literature Cited

- Addicott, W. O. (1972). Provincial middle and late Tertiary molluscan stages, Temblor Range, California. In *Proceedings of the Pacific Coast Miocene Biostratigraphic Symposium*, pages 1–26. SEPM Society for Sedimentary Geology.
- Barth, A. P., Wooden, J. L., and Coleman, D. S. (2001). SHRIMP-RG U-Pb zircon geochronology of Mesoproterozoic metamorphism and plutonism in the southwesternmost United States. *The Journal of Geology*, 109(3):319–327.
- Barth, A. P., Wooden, J. L., Tosda, R. M., Morrison, J., Dawson, D. L., and Hernly, B. M. (1995). Origin of gneisses in the aureole of the San Gabriel anorthosite complex and implications for the Proterozoic crustal evolution of southern California. *Tectonics*, 14(3):736–752.
- Black, L. P., Kamo, S. L., Allen, C. M., Davis, D. W., Aleinikoff, J. N., Valley, J. W., Mundil, R., Campbell, I. H., Korsch, R. J., Williams, I. S., and Foudoulis, C. (2004). Improved $^{206}\text{Pb}/^{238}\text{U}$ microprobe geochronology by the monitoring of a trace-element-related matrix effect; SHRIMP, ID-TIMS, ELA-ICP-MS and oxygen isotope documentation for a series of zircon standards. *Chemical Geology*, 205(1–2):115–140.
- Blake, G. H. (1983). Benthic foraminiferal paleoecology and biostratigraphy of the Vaqueros Formation, Big Mountain area, Ventura County, California. In Squires, R. R. and Filewicz, M. V., editors, *Cenozoic Geology of the Simi Valley Area, Southern California*. Pacific Section, SEPM Society for Sedimentary Geology.
- Blundell, M. C. (1983). Depositional Environments of the Vaqueros Formation, Big Mountain Area, Ventura County California. pages 161–172.

- Bohannon, R. G. (1975). Mid-Tertiary conglomerates and their bearing on transverse range tectonics, Southern California. *California Division of Mines and Geology Special Report Number 118*, pages 75–82.
- Coffey, K. T., Ingersoll, R. V., and Schmitt, A. K. (2019). Stratigraphy, provenance, and tectonic significance of the Punchbowl block, San Gabriel Mountains, California, USA. *Geosphere*, 15(2):479–501.
- Crowell, J. C. (1954). Strike-slip displacement of the San Gabriel fault, southern California. *Geology of Southern California*, 170:49–52.
- Crowell, J. C. (1973). Problems concerning the San Andreas fault system in southern California. In Kovach, R. L. and Nur, A., editors, *Proceedings of the Conference on Tectonic Problems of the San Andreas Fault System*, pages 125–135.
- Crowell, J. C. (1982). The Tectonics of Ridge Basin, Southern California. In Crowell, J. C. and Link, M. H., editors, *The Tectonics of Ridge Basin, Southern California*, pages 25–42. Pacific Section, SEPM Society for Sedimentary Geology.
- Crowell, J. C. (2003). Tectonics of Ridge Basin region, southern California. In Crowell, J. C., editor, *Evolution of Ridge Basin, Southern California: An Interplay Of Sedimentation And Tectonics*, pages 157–204. Geological Society of America Special Papers 367.
- Dibblee, T. W. (1989). Mid-Tertiary conglomerates and sandstones on the margins of the Ventura and Los Angeles basins and their tectonic significance. In Minch, J. A., Abbott, P. L., and Colburn, I. P., editors, *Conglomerates In Basin Analysis: A Symposium Dedicated to A. O. Woodford*, pages 207–226. Pacific Section, SEPM Society for Sedimentary Geology 62.
- Dibblee, T. W. (2010). *Geologic map of the Cobblestone Mountain Quadrangle, Ventura and Los Angeles counties, California: Dibblee Geology Center Map #DF-62: First Printing, 1996: Second Printing, 2010*. Santa Barbara Museum of Natural History, <http://www.sbnature.org/>.
- Edwards, L. N. (1971). *Geology of the Vaqueros and Rincon Formations, Santa Barbara Embayment, California*. University of California, Santa Barbara.
- Ehler, K. W. (1982). Basin analysis of the Miocene Mint Canyon Formation, southern California. In Ingersoll, R. V. and Woodburne, M. O., editors, *Cenozoic Nonmarine Deposits of California and Arizona*, pages 51–64. Pacific Section, Society of Economic Paleontologists and Mineralogists (SEPM).
- Ehlig, P. L. and Crowell, J. C. (1982). Mendenhall Gneiss and anorthosite-related rocks bordering Ridge Basin, southern California.
- Frizzell Jr, V. A. and Weigand, P. W. (1993). Whole-rock K-Ar ages and geochemical data from middle Cenozoic rocks, southern California: A test of correlations across the San Andreas fault. In Powell, R. D., Weldon II, R. J., and Matti, J. C., editors, *The San Andreas Fault System: Displacement, Palinspastic Reconstruction, And Geologic Evolution*, pages 273–288. Geological Society of America Memoir 178.
- Hamlin, H. (1904). *Water Resources of the Salinas Valley, California*. USGS, Water-Supply and Irrigation Paper 89.
- Hendrix, E. D. and Ingersoll, R. V. (1987). Tectonics and alluvial sedimentation of the upper Oligocene/lower Miocene Vasquez Formation, Soledad basin, southern California. *GSA Bulletin*, 98(6):647–663.
- Hoyt, J. F., Coffey, K. T., Ingersoll, R. V., and Jacobson, C. E. (2018). Paleogeographic and paleotectonic setting of the middle Miocene Mint Canyon and Caliente formations, southern California: An integrated provenance study. In Ingersoll, R. V., Lawton, T. F., and Graham, S. A., editors, *Tectonics, Sedimentary Basins, and Provenance: A Celebration of the Career of William R. Dickinson*, pages 463–480. Geological Society of America Special Paper 540.
- Ingersoll, R. V., Pratt, M. J., Davis, P. M., Caracciolo, L., Day, P. P., Hayne, P. O., Petrizzo, D. A., Gingrich, D. A., Cavazza, W., Critelli, S., Diamond, D. S., Coffey, K. T., Stang, D. M., Hoyt, J. F., Reith, R. C., and Hendrix, E. D. (2014). Paleotectonics of a complex Miocene half graben formed above a detachment fault: The Diligencia basin, Orocochia Mountains, southern California. *Lithosphere*, 6(3):157–176.
- Ingersoll, R. V. and Rumelhart, P. E. (1999). Three-stage evolution of the Los Angeles basin, southern California. *Geology*, 27(7):593–596.
- Ingersoll, R. V., Spafford, C. D., Jacobson, C. E., Grove, M., Howard, J. L., Hourigan, J., and Pedrick, J. (2018). Provenance, paleogeography and paleotectonic implications of the mid-Cenozoic Sespe Formation, coastal southern California, USA. In Ingersoll, R. V., Lawton, T. F., and Graham, S. A., editors, *Tectonics, Sedimentary Basins, and Provenance: A Celebration of the Career of William R. Dickinson*, pages 441–462. Geological Society of America Special Paper 540.
- Jacobson, C. E., Barth, A. P., and Grove, M. (2000). Late Cretaceous protolith age and provenance of the Pelona and Orocochia Schists, southern California: Implications for evolution of the Cordilleran margin. *Geology*, 28(3):219–222.
- Loel, W. and Corey, W. H. (1932). *The Vaqueros Formation, lower Miocene of California*.
- Malkowski, M. A., Sharman, G. R., Johnstone, S. A., Grove, M. J., Kimbrough, D. L., and Graham, S. A. (2019). Dilution and propagation of provenance trends in sand and mud: Geochemistry and detrital zircon geochronology of modern sediment from central California (USA). *American Journal of Science*, 319(10):846–902.
- Matti, J. C. and Morton, D. M. (1993). Paleogeographic evolution of the San Andreas fault in southern California: A reconstruction based on a new cross-fault correlation. In Powell, R. E., Weldon, R. J., and Matti, J. C., editors, *The San Andreas fault system: Displacement, palinspastic reconstruction, and geologic evolution*, pages 107–160. Geological Society of America Memoir 178.
- Nourse, J. A. (2002). Middle Miocene reconstruction of the central and eastern San Gabriel Mountains, southern California, with implications for evolution of the San Gabriel fault and Los Angeles basin. In *Contributions to crustal evolution of the southwestern United States*, pages 161–186. Geological Society of America Special Paper 365.
- Powell, R. E. (1993). Balanced palinspastic reconstruction of pre-late Cenozoic paleogeology, southern California: Geologic and kinematic constraints on evolution of the San Andreas fault system. In Powell, R. D., Weldon II, R. J., and Matti, J. C., editors, *The San Andreas Fault System: Displacement, Palinspastic Reconstruction, and Geologic Evolution*, pages 1–106. Geological Society of America Memoir 178.
- Prothero, D. R. and Donohoo, L. L. (2001). Magnetic stratigraphy of the lower Miocene (early Hemingfordian) Sespe-Vaqueros Formations, Orange County, California. In Prothero, D. R., editor, *Magnetic Stratigraphy of the Pacific Coast Cenozoic*, pages 242–253. Pacific Section, SEPM Society for Sedimentary Geology, Book 91.
- Prothero, D. R., Howard, J. L., and Dozier, T. H. (1996). Stratigraphy and paleomagnetism of the upper middle Eocene to lower Miocene (Uintan to Arikareean) Sespe Formation, Ventura County, California. In Prothero, D. R. and Emry, R. J., editors, *The Terrestrial Eocene–Oligocene Transition in North America*, pages 171–188. Cambridge University Press Cambridge and New York.
- Rumelhart, P. E. and Ingersoll, R. V. (1997). Provenance of the upper Miocene Modelo Formation and subsidence analysis of the Los Angeles basin, southern California: Implications for paleotectonic and paleogeographic reconstructions. *GSA Bulletin*, 109(7):885–899.
- Saylor, J. E. and Sundell, K. E. (2016). Quantifying comparison of large detrital geochronology data sets. *Geosphere*, 12(1):203–220.
- Sharman, G. R. and Johnstone, S. A. (2017). Sediment unmixing using detrital geochronology. *Earth and Planetary Science Letters*, 477:183–194.
- Silverman, B. W. (2018). *Density Estimation for Statistics and Data Analysis*. Routledge.
- Sláma, J., Košler, J., Condon, D. J., Crowley, J. L., Gerdes, A., Hanchar, J. M., Horstwood, M. S. A., Morris, G. A., Nasdala, L., Norberg, N., Schaltegger, U., Schoene, B., Tubrett, M. N., and Whitehouse, M. J. (2008). Plešovice zircon—A new natural reference material for U-Pb and Hf isotopic microanalysis. *Chemical Geology*, 249:1–35.
- Stanley, R. G., Cotton, M. L., Bukry, D., Filewicz, M. V., Valin, Z. C., and Vork, D. R. (1994). Stratigraphic revelations regarding the Rincon Shale (lower Miocene) in the Santa Barbara coastal area. *AAPG Bulletin*, 78(4):675–676.
- Thorup, R. R. (1943). Type locality of the Vaqueros formation. *California Division of Mines Geological Bulletin*, 118:463–466.
- Turner, D. L. and Campbell, R. H. (1979). Age of the Conejo Volcanics. In Campbell, R. F. and Yerkes, R. H., editors, *Stratigraphic Nomenclature of the Central Santa Monica Mountains, Los Angeles County, California*, pages E18–E22. Geological Survey Bulletin 1457–E.
- Vermeesch, P. (2013). Multi-sample comparison of detrital age distributions. *Chemical Geology*, 341:140–146.

- Weigand, P. W., Savage, K. L., Nicholson, C., and Barth, A. (2002). The Conejo Volcanics and other Miocene volcanic suites in southwestern California. pages 187–204. Geological Society of America Special Papers 365.
- Wiedenbeck, M., Allé, P., Corfu, F., Griffin, W. L., Meier, M., Oberli, F., von Quadt, A., Roddick, J. C., and Spiegel, W. (1995). Three natural zircon standards for U-Th-Pb, Lu-Hf, trace element and REE analyses. *Geostandards newsletter*, 19(1):1–23.
- Woodburne, M. O. (1975). Constraints for Late Cenozoic offset on the San Andreas fault system, southern California: Sedimentary basins of the Transverse Ranges and adjacent areas. In Woodburne, M. O., editor, *Cenozoic Stratigraphy of the Transverse Ranges and Adjacent Areas, Southern California*, pages 1–91.
- Yeats, R. S. (2001). Neogene tectonics of the east Ventura and San Fernando basins, California: An overview. In Wright, T. L. and Yeats, R. S., editors, *Geology and Tectonics of the San Fernando Valley and East Ventura Basin, California*, pages 9–36. Pacific Section of American Association of Petroleum Geologists Guidebook GB 77.
- Yeats, R. S., Huftile, G. J., and Stitt, L. T. (1994). Late Cenozoic tectonics of the east Ventura basin, Transverse Ranges, California. *AAPG Bulletin*, 78(7):1040–1074.
- Yeats, R. S. and Stitt, L. T. (2003). Ridge Basin and San Gabriel fault in the Castaic Lowland, southern California. In *Evolution of Ridge Basin, Southern California: An Interplay of Sedimentation and Tectonics*. Geological Society of America Special Paper 367.

TSR **The** **Sedimentary Record**

SEPM | Society for Sedimentary Geology

The Sedimentary Record (TSR) is published quarterly by SEPM. It contains peer-reviewed science articles on topics of broad and current interest to the membership of SEPM, including all aspects of sedimentology, stratigraphy, geomorphology, sedimentary geochemistry, paleontology, paleoclimatology, paleogeography, etc. We welcome high-quality, short-format scientific contributions from members of the sedimentary geoscience community.